MATERIALS PHYSICS AND MECHANICS RESEARCH ARTICLE

**Submitted: August 5, 2025** **Revised: October 20, 2025** **Accepted: November 10, 2025**

# Elastodynamic response of photothermoelastic plate with moisture due to various sources

**R. Kumar [1], N. Sharma [2], V. Rani [2]✉**

[1] Kurukshetra University, Kurukshetra, India

[2] Maharishi Markandeshwar (Deemed to be University), Mullana-Ambala, India

✉ vineeta.jaglan@gmail.com

**ABSTRACT**

This current study examines how carrier density and moisture sources cause deformation in an isotropic photothermoelastic moisture plate. We develop simplified two-dimensional equations describing the interaction of heat, moisture, and charge carriers within the material. These equations are expressed in a dimensionless form and solved analytically using Laplace and Fourier transformations to obtain the main field quantities—displacement, stress, temperature, carrier density, and moisture distribution. The theoretical results are validated for silicon material and illustrated graphically. The analysis demonstrates that both carrier density and moisture significantly affect the stress, temperature, and carrier concentration within the plate. Moisture tends to stabilize stress variations and reduce temperature fluctuations, while relaxation times strongly influence oscillation patterns in all field quantities. These results underscore the integrated role of thermal, moisture, and photoelastic effects in shaping the mechanical behavior of semiconducting materials. The proposed model aids in analyzing coupled thermoelastic, moisture, and carrier effects in semiconductors, offering improved prediction of transient responses essential for enhancing thermal stability and reliability in electronic and photonic devices.

**KEYWORDS**

isotropic • photothermoelastic • Laplace transform • Fourier transform • carrier density source •moisture source

**Citation:** Kumar R, Sharma N, Rani V. Elastodynamic response of photothermoelastic plate with moisture due to various sources. *Materials Physics and Mechanics*. 2025;53(6): 145–163.
http://dx.doi.org/10.18149/MPM.5362025_11

## Introduction

Advances in modern technology have considerably expanded the use of semiconducting materials in diverse engineering and applied physics applications. The study of wave propagation in semiconducting media is of both academic and technological significance owing to its relevance to optoelectronic and thermomechanical processes. In recent years, the photothermal excitation of short elastic pulses has become a central topic of research, finding applications in photoacoustic microscopy, thermal wave imaging, thermoelastic parameter determination, non-destructive device evaluation, laser drilling monitoring, and laser-induced annealing and melting phenomena in semiconductors. When a laser beam irradiates a semiconductor surface, part of the absorbed energy excites electrons to higher energy states. The recombination of electron–hole pairs through non-radiative transitions produces photoexcited free carriers that influence the local thermal and elastic fields. Consequently, photothermal (PT) and photoacoustic (PA) techniques have emerged as powerful diagnostic tools for investigating the internal dynamics of semiconductor materials.


Publisher: Peter the Great St. Petersburg Polytechnic University

Over the last few decades, PA and PT methods have evolved into highly sensitive and versatile techniques for characterizing semiconductors and microelectronic structures. These methods exhibit excellent sensitivity to the kinetics of photoexcited carriers and have been employed for precise analysis of carrier transport, recombination, and diffusion mechanisms (Mandelis [1]; Almond and Patel [2]; Nikolic and Todorović [3]; Mandelis and Michaelian [4]). In most semiconductor systems, an absorbed modulated laser beam generates electron-hole pairs, producing carrier-diffusion or plasma waves that significantly contribute to the PT and PA responses. These plasma waves induce periodic thermal and elastic disturbances, resulting in coupled thermoelastic and plasma wave propagation. The subsequent deformation of the crystal lattice alters the potential profiles of the conduction and valence bands, producing complex photo-induced mechanical behavior. Todorović [5–7] proposed theoretical models that linked carrier recombination and transport phenomena with the deformation and mechanical response of semiconductor media.

Considerable theoretical developments have since been made in the field of generalized thermoelasticity and its extensions. Sharma [8] examined boundary value problems in generalized thermodiffusive elastic media, while Sharma et al. [9] obtained the fundamental solution for electro-microstretch viscoelastic solids and explored wave motion. Othman et al. [10] analyzed magneto-thermoelastic behavior in perfectly conducting half-spaces subjected to magnetic and thermal fields, and Marin et al. [11] extended Saint-Venant's principle to micropolar thermoelastic diffusion models. Zenkour and Abbas [12] utilized the Green–Naghdi model to investigate thermal shock in fiber-reinforced anisotropic media under magnetic influence. Lotfy [13] applied a two-temperature model to study magneto-thermoelastic interactions, while Sharma and Sharma [14] and Abbas et al. [15] extended these formulations to bio-heat transfer and microstretch elastic media.

Further research integrated electromagnetic, fractional, and relaxation phenomena into photothermal and magneto-thermoelastic analyses. Hobiny and Abbas [16,17] employed the coupled thermoelastic–plasma wave theory using the Green–Naghdi framework and its fractional-order extensions. Marin et al. [18] developed porothermoelastic models using fractional calculus and thermal relaxation parameters. Lotfy et al. [19] and Abbas [20,21] studied the combined effects of electromagnetic, thermal, and photonic fields on semiconductor response to laser-induced heating. Recent studies by Sharma and Kumar [22,23], Lotfy et al. [24], and Mahdy et al. [25] examined photothermoelastic deformations caused by inclined loads, ramp-type heating, Hall currents, and time-fractional heat conduction effects.

Sharma and Khator [26,27] explored renewable energy challenges and microgrid planning for prosumer markets, while several studies advanced semiconductor thermoelastic modeling: Lotfy [28] studied Hall current and microtemperature effects in magneto-thermoelastic semiconductors; Hobiny et al. [29] examined wave propagation using the hyperbolic two-temperature model; El-Sapa et al. [30] applied a nonlocal variable-conductivity approach at the nanoscale; Raddadi et al. [31] modeled photoacoustic wave generation via carrier diffusion; and Sharma et al. [32] investigated micropolar thermoviscoelasticity incorporating nonlocal and hyperbolic two-temperature effects under the MGT framework.

The coupling of heat and moisture diffusion known as hygro-thermoelasticity has also received significant attention due to its relevance in porous and hygroscopic materials such as composites, foams, biotissues, and concrete. Foundational studies by Szekeres [33,34] and Szekeres and Engelbrecht [35] established analogies between heat and moisture transfer, later expanded by Sih et al. [36] to analyze coupled hygro-thermoelastic behavior. More recently, Alhashash et al. [37] and El-Sapa et al. [38] developed mathematical–physical models describing the effects of moisture diffusivity in semiconducting media under two-temperature and nonlocal frameworks. Lotfy et al. [39] and Alshehri and Lotfy [40] investigated the interaction between photoacoustic waves and moisture diffusivity in hydro-poroelastic semiconductors.

Kumar and Devi [41] and Kumar et al. [42,43] investigated thick circular plates through modified couple stress and photothermoelastic frameworks, considering factors such as porosity, phase lag, and fractional behavior. Abbas et al. [44,45] and Lotfy et al. [46] explored thermoelastic half-spaces incorporating diffusion, voids, and Hall current influences. Alzahrani and Abbas [47] and Sharma et al. [48] analyzed semiconductor half-spaces exhibiting nonlocal and phase-lag thermoelastic responses.

The novelty of the present work lies in the combined analysis of carrier density and moisture diffusivity effects on the deformation of an isotropic photothermoelastic moisture (IPTM) plate, an aspect that has not been extensively reported in prior literature. Unlike earlier studies that focused separately on thermal or photothermal interactions, the current formulation incorporates simultaneous contributions from carrier generation, moisture transport, and relaxation mechanisms. The governing field equations are derived using generalized thermoelasticity and diffusion theories, introducing suitable non-dimensional parameters and potential functions to simplify the coupled system. The equations are solved analytically using Laplace and Fourier transform techniques to obtain expressions for temperature, carrier density, moisture concentration, and normal stress. The results are numerically inverted to retrieve time-domain responses, and graphical analyses are presented to demonstrate the effects of carrier density, moisture diffusivity, and relaxation times on the deformation characteristics of the IPTM plate, which offers novel perspectives on the multiphysical coupling mechanisms in semiconductor materials.

## Basic equations

Following the formulations of Todorovic [5–7], Szekeres [33,34], and Alenazi et al. [49], the constitutive relations and field equations are developed for a homogeneous, isotropic, and linearly elastic photothermoelastic material with moisture. The model neglects body forces, carrier photogeneration, and internal heat or moisture sources, while incorporating finite relaxation effects for heat, carrier, and moisture diffusion.

$$t_{ij} = 2\mu e_{ij} + \delta_{ij}(\lambda e_{kk} - \gamma_t T - \gamma_n N - \gamma_m M), \tag{1}$$

$$\left(2\mu e_{ij,j} + \lambda e_{kk,i} - \gamma_t T_{,i} - \gamma_n N_{,i} - \gamma_m M_{,i}\right) + F_i = \rho \frac{\partial^2 u_i}{\partial t^2}, \tag{2}$$

$$D_e N_{,ii} - \frac{\partial N}{\partial t} - \frac{N}{\tau} + \delta \frac{T}{\tau} = 0, \tag{3}$$

$$\rho C_e\left(D_t T_{,ii} + D_t^m M_{,ii}\right) + \frac{E_g N}{\tau} = \left(1 + \tau_o \frac{\partial}{\partial t}\right)\left[\rho C_e \dot{T} + \gamma_t T_o \dot{e}_{kk}\right], \tag{4}$$

$$K_m\left(D_m M_{,ii} + D_m^t T_{,ii}\right) + \frac{E_g N}{\tau} = \left(1 + \tau^o \frac{\partial}{\partial t}\right)\left[K_m \dot{M} + \gamma_m D_m M_o \dot{e}_{kk}\right]. \quad (5)$$

where $t_{ij}$ are components of stress tensor; $e_{ij}$ are components of strain tensor, $\lambda$ end $\mu$ are Lame's constants, $\delta_{ij}$ is kronecker delta, $\gamma_t = (3\lambda + 2\mu)\alpha_t - \alpha_t$ are linear thermal expansion coefficients, $\gamma_n = (3\lambda + 2\mu)\alpha_n - \alpha_n$ are electronic deformation coefficients, $\gamma_m = (3\lambda + 2\mu)\alpha_m - \alpha_m$ are moisture expansion coefficients, $F_i$ are the components of body force per unit volume, $u_i$ are components of displacement, $\rho$ is the medium density, $D_e$ are the coefficients of carrier diffusion; $N = n\text{-}n_0$, $n_0$ are the carrier concentration at equilibrium, $\tau$ is the photogenerated carrier lifetime, $\delta = \frac{\partial n_0}{\partial T}$ is thermal activation coupling parameter, $T$ is the temperature distribution, $C_e$ is the specific heat, $D_t = K/\rho C_e$ is temperature diffusivity, where $K$ is a coefficient of thermal conductivity, $D_t^m$ is coupled moisture diffusivity, $E_g$ is the semiconductor energy gap, $\tau_o$is the thermal relaxation time, $\tau^o$ is the moisture relaxation time, $T_0$ is the reference temperature, $K_m$ is moisture diffusion constant, $D_m$ is moisture diffusivity, $D_m^t$ is coupled thermal diffusivity, $M_0$ is the reference moisture. Partial derivatives and time derivatives are denoted by the symbols "," and "." respectively.

## Formulation of the problem and model assumptions

We investigate a homogeneous, isotropic, thermally conducting, infinite photothermoelastic moisture Cartesian plate with finite thickness 2d having an initial uniform temperature $T_o$. The origin of the coordinate system may be any point on the middle plane, and the middle plane of the plate coincides with the $x_1x_2$-plane, consequently $-d \le x_3 \le d$ and $-\infty < x_1, x_2 < \infty$. The boundary surface of the plate is subjected to carrier density source and moisture source. We limit our analysis to the $x_1x_3$-plane, which we assume the plane of incident, so that the physical field elements vary with $x_1, x_3, t$. Consequently, displacement components, temperature distribution, carrier density distribution and moisture distribution are provided by:

$$\vec{u} = \left(u_1(x_1, x_3, t), 0, u_3(x_1, x_3, t)\right), T = T(x_1, x_3, t), N = N(x_1, x_3, t), M = M(x_1, x_3, t). \quad (6)$$

The governing Eqs. (2)–(5) and constitutive relation (1) for IPTM plate utilizing Eq. (6), adopt the following form:

$$(\lambda + \mu)\frac{\partial e}{\partial x_1} + \mu \Delta u_1 - \gamma_t \frac{\partial T}{\partial x_1} - \gamma_n \frac{\partial N}{\partial x_1} - \gamma_m \frac{\partial M}{\partial x_1} = \rho \frac{\partial^2 u_1}{\partial t^2}, \quad (7)$$

$$(\lambda + \mu)\frac{\partial e}{\partial x_3} + \mu \Delta u_3 - \gamma_t \frac{\partial T}{\partial x_3} - \gamma_n \frac{\partial N}{\partial x_3} - \gamma_m \frac{\partial M}{\partial x_3} = \rho \frac{\partial^2 u_3}{\partial t^2}, \quad (8)$$

$$D_e \Delta N - \frac{\partial N}{\partial t} - \frac{N}{\tau} + \delta \frac{T}{\tau} = 0, \quad (9)$$

$$\rho C_e [D_t \Delta T + D_t^m \Delta M] + \frac{E_g N}{\tau} = \left(1 + \tau_o \frac{\partial}{\partial t}\right)\left[\rho C_e \frac{\partial T}{\partial t} + \gamma_t T_o \frac{\partial e}{\partial t}\right], \quad (10)$$

$$K_m [D_m \Delta M + D_m^t \Delta T] + \frac{E_g N}{\tau} = \left(1 + \tau^o \frac{\partial}{\partial t}\right)\left[K_m \frac{\partial M}{\partial t} + \gamma_m D_m M_o \frac{\partial e}{\partial t}\right], \quad (11)$$

$$t_{11} = (\lambda + 2\mu)\frac{\partial u_1}{\partial x_1} + \lambda \frac{\partial u_3}{\partial x_3} - \gamma_t T - \gamma_n N - \gamma_m M, \quad (12)$$

$$t_{33} = (\lambda + 2\mu)\frac{\partial u_3}{\partial x_3} + \lambda \frac{\partial u_1}{\partial x_1} - \gamma_t T - \gamma_n N - \gamma_m M, \quad (13)$$

$$t_{31} = \mu\left(\frac{\partial u_1}{\partial x_3} + \frac{\partial u_3}{\partial x_1}\right), \quad (14)$$

where $e = \frac{\partial u_1}{\partial x_1} + \frac{\partial u_3}{\partial x_3}$ and $\Delta = \frac{\partial^2}{\partial x_1^2} + \frac{\partial^2}{\partial x_3^2}$ .

The model is formulated under the following physical and mathematical assumptions:

The plate is homogeneous, isotropic, and linearly elastic, with uniform mechanical, thermal, and electronic properties. All field variables temperature, carrier density, and moisture concentration are considered small perturbations around a uniform equilibrium state, allowing the governing equations to be linearized. Finite relaxation times are incorporated for heat, carrier, and moisture fluxes to represent finite-speed propagation and realistic transient behavior. Body forces, carrier photogeneration, and internal heat or moisture sources within the medium are neglected.

The problem is treated as two-dimensional, assuming no variation along the $x_2$-axis, and all field variables are continuous and differentiable, ensuring the applicability of Laplace and Fourier transforms. The plate is initially stress-free and thermally uniform, and its bounding surfaces are subjected to prescribed, time-dependent carrier-density and moisture loadings.

The dimensionless quantities are defined in the following way:

$$(x_1', x_3', u_1', u_3') = \eta_1 C_o (x_1, x_3, u_1, u_3),\ (t_{11}', t_{33}', t_{31}') = \frac{1}{\lambda+2\mu}(t_{11}, t_{33}, t_{31}),$$
$$\left(t', \tau_o', \tau^{o\prime}\right) = \eta_1 C_o^2 (t, \tau_o, \tau^o),\ T' = \frac{\gamma_t}{\lambda+2\mu} T, \tag{15}$$
$$N' = \frac{\gamma_n}{\lambda+2\mu} N,\ e' = e\ ,\ M' = M,$$

where $\eta_1 = \frac{\rho C_e}{K}, C_o^2 = \frac{\lambda+2\mu}{\rho}$.

Using the dimensionless quantities provided by Eq. (15) in Eqs. (7)–(14) and, after prime deprivation, we obtain:

$$f_{11}\frac{\partial e}{\partial x_1} + f_{12}\Delta u_1 - \frac{\partial T}{\partial x_1} - \frac{\partial N}{\partial x_1} - f_{13}\frac{\partial M}{\partial x_1} = \frac{\partial^2 u_1}{\partial t^2}, \tag{16}$$

$$f_{11}\frac{\partial e}{\partial x_3} + f_{12}\Delta u_3 - \frac{\partial T}{\partial x_3} - \frac{\partial N}{\partial x_3} - f_{13}\frac{\partial M}{\partial x_3} = \frac{\partial^2 u_3}{\partial t^2}, \tag{17}$$

$$\Delta N - f_{14}\frac{\partial N}{\partial T} - f_{15}N + f_{16}T = 0, \tag{18}$$

$$\Delta T + f_{17}\Delta M + f_{18}N = \left(1 + \tau_o \frac{\partial}{\partial t}\right)\left[f_{19}\frac{\partial T}{\partial t} + f_{20}\frac{\partial e}{\partial t}\right], \tag{19}$$

$$\Delta M + f_{21}\Delta T + f_{22}N = \left(1 + \tau^o \frac{\partial}{\partial t}\right)\left[f_{23}\frac{\partial M}{\partial t} + f_{24}\frac{\partial e}{\partial t}\right], \tag{20}$$

$$t_{11} = \frac{\partial u_1}{\partial x_1} + f_{25}\frac{\partial u_3}{\partial x_3} - T - N - f_{13}M, \tag{21}$$

$$t_{33} = \frac{\partial u_3}{\partial x_3} + f_{25}\frac{\partial u_1}{\partial x_1} - T - N - f_{13}M, \tag{22}$$

$$t_{31} = f_{12}\left(\frac{\partial u_1}{\partial x_3} + \frac{\partial u_3}{\partial x_1}\right), \tag{23}$$

where $f_{11} = \frac{\lambda+\mu}{\rho C_o^2}$, $f_{12} = \frac{\mu}{\rho C_o^2}$, $f_{13} = \frac{\gamma_m}{\rho C_o^2}$, $f_{14} = \frac{1}{\eta_1 D_e}$, $f_{15} = \frac{1}{D_e \eta_1^2 C_o^2 \tau}$, $f_{16} = \frac{\delta\gamma_n}{D_e \tau \gamma_t \eta_1^2 C_o^2}$,
$f_{17} = \frac{D_t^m \gamma_t}{D_t(\lambda+2\mu)}$, $f_{18} = \frac{E_g \gamma_t}{\tau\gamma_n \rho C_e D_t \eta_1^2 C_o^2}$, $f_{19} = \frac{1}{D_t \eta_1}$, $f_{20} = \frac{\gamma_t^2 T_o}{\rho C_e D_t \eta_1 (\lambda+2\mu)}$, $f_{21} = \frac{D_m^t(\lambda+2\mu)}{D_m \gamma_t}$,
$f_{22} = \frac{E_g(\lambda+2\mu)}{\tau\gamma_n K_m D_m \eta_1^2 C_o^2}$, $f_{23} = \frac{1}{D_m \eta_1}$, $f_{24} = \frac{\gamma_m M_o}{K_m \eta_1}$, $f_{25} = \frac{\lambda}{\lambda+2\mu}$.

According to Helmholtz's decomposition, $u_1$ and $u_3$ have the following non-dimensional connections to the potential functions $\Phi$ and $\Psi$:

$$u_1 = \frac{\partial \Phi}{\partial x_1} - \frac{\partial \Psi}{\partial x_3},\ u_3 = \frac{\partial \Phi}{\partial x_3} + \frac{\partial \Psi}{\partial x_1}. \tag{24}$$

With the assistance of Eq. (24), Eqs. (16)–(17) provide:

$$\left(\Delta - \frac{\partial^2}{\partial t^2}\right)\Phi - T - N - f_{13}M = 0, \tag{25}$$

$$\Delta\Psi - \frac{1}{f_{12}}\frac{\partial^2 \Psi}{\partial t^2} = 0. \tag{26}$$

Define Laplace and Fourier Transform as:

$$\hat{f}(x_1, x_3, \mathfrak{s}) = \int_0^\infty f(x_1, x_3, t) e^{-\mathfrak{s}t} dt, \tag{27}$$

$$\tilde{f}(\xi, x_3, \mathfrak{s}) = \int_{-\infty}^\infty \hat{f}(x_1, x_3, \mathfrak{s}) e^{i\xi x_1} dx_1, \tag{28}$$

where $\mathfrak{s}$ is Laplace transform parameter and $\xi$ is Fourier transform parameter.

After executing Laplace and Fourier transforms provided by Eqs. (27)–(28) to Eqs. (25), *(18)–(20)* and (26), we obtain the following:

$$\left(-\xi^2 + \frac{d^2}{dx_3^2} - \mathfrak{s}^2\right)\widetilde{\Phi} - \tilde{T} - \tilde{N} - f_{13}\widetilde{M} = 0, \tag{29}$$

$$\left(-\xi^2 + \frac{d^2}{dx_3^2}\right)\tilde{N} - f_{14}\mathfrak{s}\tilde{N} - f_{15}\tilde{N} + f_{16}\tilde{T} = 0, \tag{30}$$

$$-\xi^2\tilde{T} + \frac{d^2\tilde{T}}{dx_3^2} + f_{17}\left(-\xi^2\tilde{M} + \frac{d^2\tilde{M}}{dx_3^2}\right) + f_{18}\tilde{N} = (1 + \tau_o\mathfrak{s})\left[f_{19}\mathfrak{s}\tilde{T} + f_{20}\mathfrak{s}\left(-\xi^2 + \frac{d^2}{dx_3^2}\right)\widetilde{\Phi}\right], \tag{31}$$

$$-\xi^2\widetilde{M} + \frac{d^2\tilde{M}}{dx_3^2} + f_{21}\left(-\xi^2\tilde{T} + \frac{d^2\tilde{T}}{dx_3^2}\right) + f_{22}\tilde{N} = (1 + \tau^o\mathfrak{s})\left[f_{23}\mathfrak{s}\widetilde{M} + f_{24}\mathfrak{s}\left(-\xi^2 + \frac{d^2}{dx_3^2}\right)\widetilde{\Phi}\right], \tag{32}$$

$$\left[\left(-\xi^2 + \frac{d^2}{dx_3^2}\right) - \frac{1}{f_{12}}\mathfrak{s}^2\right]\widetilde{\Psi} = 0. \tag{33}$$

Employing transforms defined by Eqs. (27)–(28) on Eqs. (24) and (21)–(23), the displacement and stress components are obtained as follows:

$$\tilde{u}_1 = -i\xi\widetilde{\Phi} - \frac{d\widetilde{\Psi}}{dx_3}, \tag{34}$$

$$\tilde{u}_3 = \frac{d\widetilde{\Phi}}{dx_3} - i\xi\widetilde{\Psi}, \tag{35}$$

$$\tilde{t}_{11} = -i\xi\tilde{u}_1 + f_{25}\frac{d\tilde{u}_3}{dx_3} - \tilde{T} - \tilde{N} - f_{13}\widetilde{M}, \tag{36}$$

$$\tilde{t}_{33} = \frac{d\tilde{u}_3}{dx_3} - i\xi f_{25}\tilde{u}_1 - \tilde{T} - \tilde{N} - f_{13}\widetilde{M}, \tag{37}$$

$$\tilde{t}_{31} = f_{12}\left(\frac{d\tilde{u}_1}{dx_3} - i\xi\tilde{u}_3\right). \tag{38}$$

Algebraic simplifications of Eqs. (29)–(32) result in:

$$(\mathfrak{B}_1 D^8 + \mathfrak{B}_2 D^6 + \mathfrak{B}_3 D^4 + \mathfrak{B}_4 D^2 + \mathfrak{B}_5)\left(\widetilde{\Phi}, \tilde{T}, \tilde{N}, \widetilde{M}\right) = 0, \tag{39}$$

where $D = \frac{d}{dx_3}$, $\mathfrak{B}_1 = f_{17}f_{21} - 1$, $\mathfrak{B}_2 = \mathfrak{R}_1 + \mathfrak{R}_4 - \mathfrak{B}_1\xi^2 - \mathfrak{B}_1\mathfrak{s}^2 + f_{13}\mathfrak{R}_{11}$,

$\mathfrak{B}_3 = \mathfrak{R}_2 - \mathfrak{R}_1\xi^2 - \mathfrak{R}_1\mathfrak{s}^2 + \mathfrak{R}_5 - \mathfrak{R}_8 + f_{13}\mathfrak{R}_{12}$,

$\mathfrak{B}_4 = \mathfrak{R}_3 - \mathfrak{R}_2\xi^2 - \mathfrak{R}_2\mathfrak{s}^2 + \mathfrak{R}_6 - \mathfrak{R}_9 + f_{13}\mathfrak{R}_{13}$,

$\mathfrak{B}_5 = -\mathfrak{R}_3\xi^2 - \mathfrak{R}_3\mathfrak{s}^2 + \mathfrak{R}_7 - \mathfrak{R}_{10} + f_{13}\mathfrak{R}_{14}$,

and

$\mathfrak{R}_1 = (3 - 3f_{17}f_{21})\xi^2 + f_{19}r_1 + f_{23}r_2 + f_{14}\mathfrak{s} + f_{15} - f_{14}f_{17}f_{21}\mathfrak{s} - f_{15}f_{17}f_{21}$,

$\mathfrak{R}_2 = 3f_{17}f_{21}\xi^4 - 3\xi^4 + 2f_{15}f_{17}f_{21}\xi^2 + 2f_{14}f_{17}f_{21}\mathfrak{s}\xi^2 - 2f_{14}\mathfrak{s}\xi^2 - 2f_{15}\xi^2 - 2f_{19}r_1\xi^2 - -2f_{23}r_2\xi^2 - f_{14}f_{19}r_1\mathfrak{s} - f_{14}f_{23}r_2\mathfrak{s} - f_{15}f_{19}r_1 - f_{15}f_{23}r_2 - f_{19}f_{23}r_1r_2 + f_{16}f_{18} - -f_{16}f_{17}f_{22}$,

$\mathfrak{R}_3 = \xi^6 - f_{17}f_{21}\xi^6 + f_{15}\xi^4 + f_{14}\mathfrak{s}\xi^4 - f_{14}f_{17}f_{21}\mathfrak{s}\xi^4 - f_{15}f_{17}f_{21}\xi^4 + f_{19}r_1\xi^4 + f_{23}r_2\xi^4 + +f_{14}f_{19}r_1\mathfrak{s}\xi^2 + f_{14}f_{23}r_2\mathfrak{s}\xi^2 + f_{15}f_{19}r_1\xi^2 + f_{15}f_{23}r_2\xi^2 + f_{16}f_{17}f_{22}\xi^2 - f_{16}f_{18}\xi^2 + +f_{19}f_{23}r_1r_2\xi^2 + f_{14}f_{19}f_{23}r_1r_2\mathfrak{s} + f_{15}f_{19}f_{23}r_1r_2 - f_{16}f_{18}f_{23}r_2$,

$\mathfrak{R}_4 = f_{17}f_{24}r_2 - f_{20}r_1$,

$\mathfrak{R}_5 = 3f_{20}r_1\xi^2 - 3f_{17}f_{24}r_2\xi^2 + f_{14}f_{20}r_1\mathfrak{s} - f_{14}f_{17}f_{24}r_2\mathfrak{s} + f_{15}f_{20}r_1 - f_{15}f_{17}f_{24}r_2 + +f_{20}f_{23}r_1r_2$,

$\mathfrak{R}_6 = 3f_{17}f_{24}r_2\xi^4 - 3f_{20}r_1\xi^4 - 2f_{15}f_{20}r_1\xi^2 - 2f_{14}f_{20}r_1\mathfrak{s}\xi^2 - 2f_{20}f_{23}r_1r_2\xi^2 + +2f_{14}f_{17}f_{24}r_2\mathfrak{s}\xi^2 + 2f_{15}f_{17}f_{24}r_2\xi^2 - f_{14}f_{20}f_{23}r_1r_2\mathfrak{s} - f_{15}f_{20}f_{23}r_1r_2$,

$\mathfrak{R}_7 = f_{20}r_1\xi^6 - f_{17}f_{24}r_2\xi^6 + f_{14}f_{20}r_1\mathfrak{s}\xi^4 + f_{15}f_{20}r_1\xi^4 + f_{20}f_{23}r_1r_2\xi^4 - -f_{14}f_{17}f_{24}r_2\mathfrak{s}\xi^4 - f_{15}f_{17}f_{24}r_2\xi^4 + f_{14}f_{20}f_{23}r_1r_2\mathfrak{s}\xi^2 + f_{15}f_{20}f_{23}r_1r_2\xi^2$,

$\Re_8 = f_{16}f_{20}r_1 - f_{16}f_{17}f_{24}r_2,$
$\Re_9 = 2f_{16}f_{17}f_{24}r_2\xi^2 - 2f_{16}f_{20}r_1\xi^2 - f_{16}f_{20}f_{23}r_1r_2,$
$\Re_{10} = f_{16}f_{20}r_1\xi^4 - f_{16}f_{17}f_{24}r_2\xi^4 + f_{16}f_{20}f_{23}r_1r_2\xi^2,$
$\Re_{11} = f_{20}f_{21}r_1 - f_{24}r_2,$
$\Re_{12} = 3f_{24}r_2\xi^2 - 3f_{20}f_{21}r_1\xi^2 + f_{14}f_{24}r_2\mathfrak{s} - f_{14}f_{20}f_{21}r_1\mathfrak{s} + f_{15}f_{24}r_2 - f_{15}f_{20}f_{21}r_1 + +f_{19}f_{24}r_1r_2,$
$\Re_{13} = 3f_{20}f_{21}r_1\xi^4 - 3f_{24}r_2\xi^4 - 2f_{14}f_{24}r_2\mathfrak{s}\xi^2 + 2f_{14}f_{20}f_{21}r_1\mathfrak{s}\xi^2 - 2f_{15}f_{24}r_2\xi^2 + +2f_{15}f_{20}f_{21}r_1\xi^2 - 2f_{19}f_{24}r_1r_2\xi^2 - f_{14}f_{19}f_{24}r_1r_2\mathfrak{s} - f_{15}f_{19}f_{24}r_1r_2 - f_{16}f_{20}f_{22}r_1 + +f_{16}f_{18}f_{24}r_2,$
$\Re_{14} = f_{24}r_2\xi^6 - f_{20}f_{21}r_1\xi^6 - f_{14}f_{20}f_{21}r_1\mathfrak{s}\xi^4 + f_{14}f_{24}r_2\mathfrak{s}\xi^4 - f_{15}f_{20}f_{21}r_1\xi^4 + +f_{15}f_{24}r_2\xi^4 + f_{19}f_{24}r_1r_2\xi^4 + f_{14}f_{19}f_{24}r_1r_2\mathfrak{s}\xi^2 + f_{15}f_{19}f_{24}r_1r_2\xi^2 - f_{16}f_{18}f_{24}r_2\xi^2 + +f_{16}f_{20}f_{22}r_1\xi^2,$
with $r_1 = \mathfrak{s}(1 + \tau_o\mathfrak{s}),\ r_2 = \mathfrak{s}(1 + \tau^o\mathfrak{s}).$

The general solution of Eq. (39) is expressed as:

$$\left(\tilde{\Phi}, \tilde{T}, \tilde{N}, \tilde{M}\right) = \sum_{i=1}^{4}(1, \alpha_i^{\diamond}, \beta_i^{\diamond}, \gamma_i^{\diamond})\,\bar{C}_i^{\diamond}\cosh m_i^{\diamond}x_3, \tag{40}$$

where $m_i^{\diamond}(i = 1, 2, 3, 4)$ are roots of $\mathfrak{B}_1D^8 + \mathfrak{B}_2D^6 + \mathfrak{B}_3D^4 + \mathfrak{B}_4D^2 + \mathfrak{B}_5 = 0$ and the coupling parameters $\alpha_i^{\diamond}, \beta_i^{\diamond}, \gamma_i^{\diamond}$ are given by:

$$\alpha_i^{\diamond} = \sum_{i=1}^{4}\frac{\Re_4 m_i^{\diamond 6} + \Re_5 m_i^{\diamond 4} + \Re_6 m_i^{\diamond 2} + \Re_7}{\mathfrak{B}_1 m_i^{\diamond 6} + \Re_1 m_i^{\diamond 4} + \Re_2 m_i^{\diamond 2} + \Re_3}, \tag{41}$$

$$\beta_i^{\diamond} = \sum_{i=1}^{4}\frac{\Re_8 m_i^{\diamond 4} + \Re_9 m_i^{\diamond 2} + \Re_{10}}{\mathfrak{B}_1 m_i^{\diamond 6} + \Re_1 m_i^{\diamond 4} + \Re_2 m_i^{\diamond 2} + \Re_3}, \tag{42}$$

$$\gamma_i^{\diamond} = \sum_{i=1}^{4}\frac{\Re_{11} m_i^{\diamond 6} + \Re_{12} m_i^{\diamond 4} + \Re_{13} m_i^{\diamond 2} + \Re_{14}}{\mathfrak{B}_1 m_i^{\diamond 6} + \Re_1 m_i^{\diamond 4} + \Re_2 m_i^{\diamond 2} + \Re_3}. \tag{43}$$

Additionally, Eq. (33) has a solution provided by:

$$\tilde{\Psi} = \bar{C}_5^{\diamond}\sinh m_5^{\diamond}x_3, \tag{44}$$

where $m_5^{\diamond}$ is a root of equation $D^2 + \mathfrak{B}_6 = 0$, where $\mathfrak{B}_6 = -\left(\xi^2 + \frac{1}{f_{12}}\mathfrak{s}^2\right)$.

Expressions for displacement and stress components are obtained with the help of Eqs. (34)–(38), (40) and (44) as:

$$\tilde{u}_1 = -\mathrm{i}\xi\sum_{i=1}^{4}\bar{C}_i^{\diamond}\cosh m_i^{\diamond}x_3 - \bar{C}_5^{\diamond}m_5^{\diamond}\cosh m_5^{\diamond}x_3, \tag{45}$$

$$\tilde{u}_3 = \sum_{i=1}^{4}\bar{C}_i^{\diamond}m_i^{\diamond}\sinh m_i^{\diamond}x_3 - \mathrm{i}\xi\bar{C}_5^{\diamond}\sinh m_5^{\diamond}x_3, \tag{46}$$

$$\tilde{t}_{33} = \sum_{i=1}^{4}\left(m_i^{\diamond 2} - \xi^2 f_{25} - \alpha_i^{\diamond} - \beta_i^{\diamond} - f_{13}\gamma_i^{\diamond}\right)\bar{C}_i^{\diamond}\cosh m_i^{\diamond}x_3 + +\mathrm{i}\xi(f_{25} - 1)\bar{C}_5^{\diamond}m_5^{\diamond}\cosh m_5^{\diamond}x_3, \tag{47}$$

$$\tilde{t}_{11} = \sum_{i=1}^{4}\left(-\xi^2 + m_i^{\diamond 2}f_{25} - \alpha_i^{\diamond} - \beta_i^{\diamond} - f_{13}\gamma_i^{\diamond}\right)\bar{C}_i^{\diamond}\cosh m_i^{\diamond}x_3 + +\mathrm{i}\xi(f_{25} - 1)\bar{C}_5^{\diamond}m_5^{\diamond}\cosh m_5^{\diamond}x_3, \tag{48}$$

$$\tilde{t}_{31} = -2\mathrm{i}\xi\sum_{i=1}^{4}f_{12}\bar{C}_i^{\diamond}m_i^{\diamond}\sinh m_i^{\diamond}x_3 - (m_5^2 + \xi^2)\bar{C}_5^{\diamond}\sinh m_i^{\diamond}x_3. \tag{49}$$

## Boundary restrictions

The boundary restrictions for an isotropic photothermoelastic moisture plate subjected to carrier density source and moisture source are considered as:

$$\left.\begin{aligned} &t_{33} = 0,\\ &t_{31} = 0,\\ &T = 0,\\ &N = \mathrm{F}_3(x_1, x_3, t),\\ &M = \mathrm{F}_4(x_1, x_3, t), \end{aligned}\right\} \tag{50}$$

where

$$\mathrm{F}_3(x_1,x_3,t)=\mathrm{F}_{30}\delta(x_1)(\cosh x_3)H(t-a), \tag{51}$$
$$\mathrm{F}_4(x_1,x_3,t)=\mathrm{F}_{40}\delta(x_1)(\cosh x_3)\frac{\sin\pi t}{\eta}. \tag{52}$$

Here, $\delta(\,)$ is Dirac delta function, $H(\,)$ is Heaviside step function, $\mathrm{F}_{30}$ is the magnitude of the carrier density source, $\mathrm{F}_{40}$ is the constant moisture applied on the boundary.

Applying Laplace and Fourier transform defined by Eqs. (27)-(28) on Eqs. (50)–(52), we obtain:

$$\left.\begin{array}{l}\tilde{t}_{33}=0,\\ \tilde{t}_{31}=0,\\ \tilde{T}=0,\\ \widetilde{N}=\tilde{\mathrm{F}}_3(\xi,x_3,\mathfrak{s}),\\ \widetilde{M}=\tilde{\mathrm{F}}_4(\xi,x_3,\mathfrak{s}),\end{array}\right\}\ \text{at } x_3=\pm d\,, \tag{53}$$

where

$$\tilde{\mathrm{F}}_3(\xi,x_3,\mathfrak{s})=\mathrm{F}_{30}(\cosh x_3)\frac{e^{-\mathfrak{s}a}}{\mathfrak{s}}, \tag{54}$$
$$\tilde{\mathrm{F}}_4(\xi,x_3,\mathfrak{s})=\mathrm{F}_{40}(\cosh x_3)\left(\frac{\eta\pi}{\pi^2+\eta^2\mathfrak{s}^2}\right)(1+e^{-\eta\mathfrak{s}}). \tag{55}$$

Substituting the values of $\tilde{t}_{33},\tilde{t}_{31},\tilde{T},\widetilde{N},\widetilde{M}$ from Eqs. (47), (49) and (40) in the transformed boundary restrictions (53), along with Eqs. (54)–(55), yield:

$$\sum_{i=1}^{5}(a_i^{\diamond}\bar{C}_i^{\diamond}\cosh m_i^{\diamond}x_3)=0, \tag{56}$$
$$\sum_{i=1}^{5}(b_i^{\diamond}\bar{C}_i^{\diamond}\sinh m_i^{\diamond}x_3)=0, \tag{57}$$
$$\sum_{i=1}^{4}\alpha_i^{\diamond}\bar{C}_i^{\diamond}\cosh m_i^{\diamond}x_3=0, \tag{58}$$
$$\sum_{i=1}^{4}\beta_i^{\diamond}\bar{C}_i^{\diamond}\cosh m_i^{\diamond}x_3=\tilde{\mathrm{F}}_3(\xi,x_3,\mathfrak{s}), \tag{59}$$
$$\sum_{i=1}^{4}\gamma_i^{\diamond}\bar{C}_i^{\diamond}\cosh m_i^{\diamond}x_3=\tilde{\mathrm{F}}_4(\xi,x_3,\mathfrak{s}), \tag{60}$$

where $a_i^{\diamond}=m_i^{\diamond 2}-\xi^2 f_{25}-\alpha_i^{\diamond}-\beta_i^{\diamond}-f_{13}\gamma_i^{\diamond}$, $b_i^{\diamond}=-2\mathrm{i}\xi f_{12}m_i^{\diamond}$, $i=1,2,3,4$, and $a_5^{\diamond}=\mathrm{i}\xi(f_{25}-1)m_5^{\diamond}$ and $b_5^{\diamond}=-\left(m_5^{\diamond 2}+\xi^2\right)f_{12}$.

Equations (56)–(60) are expressed in matrix form as:

$$A^{\diamond}\bar{C}_i^{\diamond}=\bar{B}, \tag{61}$$

where

$$A^{\diamond}=\begin{bmatrix}a_1^{\diamond}\mathcal{C}_1 & a_2^{\diamond}\mathcal{C}_2 & a_3^{\diamond}\mathcal{C}_3 & a_4^{\diamond}\mathcal{C}_4 & a_5^{\diamond}\mathcal{C}_5\\ b_1^{\diamond}\mathcal{S}_1 & b_2^{\diamond}\mathcal{S}_2 & b_3^{\diamond}\mathcal{S}_3 & b_4^{\diamond}\mathcal{S}_4 & b_5^{\diamond}\mathcal{S}_5\\ \alpha_1^{\diamond}\mathcal{C}_1 & \alpha_2^{\diamond}\mathcal{C}_2 & \alpha_3^{\diamond}\mathcal{C}_3 & \alpha_4^{\diamond}\mathcal{C}_4 & 0\\ \beta_1^{\diamond}\mathcal{C}_1 & \beta_2^{\diamond}\mathcal{C}_2 & \beta_3^{\diamond}\mathcal{C}_3 & \beta_4^{\diamond}\mathcal{C}_4 & 0\\ \gamma_1^{\diamond}\mathcal{C}_1 & \gamma_2^{\diamond}\mathcal{C}_2 & \gamma_3^{\diamond}\mathcal{C}_3 & \gamma_4^{\diamond}\mathcal{C}_4 & 0\end{bmatrix},\ \bar{C}_i^{\diamond}=\begin{bmatrix}\bar{C}_1^{\diamond}\\ \bar{C}_2^{\diamond}\\ \bar{C}_3^{\diamond}\\ \bar{C}_4^{\diamond}\\ \bar{C}_5^{\diamond}\end{bmatrix},\ \bar{B}=\begin{bmatrix}0\\ 0\\ 0\\ \tilde{\mathrm{F}}_3(\xi,d,\mathfrak{s})\\ \tilde{\mathrm{F}}_4(\xi,d,\mathfrak{s})\end{bmatrix}, \tag{62}$$

and $\mathcal{C}_i=\cosh m_i^{\diamond}d\,,\mathcal{S}_i=\sinh m_i^{\diamond}d$.

From Eq. (62), we determine:

$$\bar{C}_i^{\diamond}=\frac{\bar{\Delta}_i^{\diamond}}{\bar{\Delta}^{\diamond}}\,,\ i=1,2,3,4,5,$$
$$\bar{\Delta}^{\diamond}=\mathcal{C}_2\mathcal{C}_3\mathcal{C}_4(b_1^{\diamond}a_5^{\diamond}\mathcal{S}_1\mathcal{C}_5-a_1^{\diamond}b_5^{\diamond}\mathcal{S}_5\mathcal{C}_1)\mathfrak{R}_{29}-\mathcal{C}_1\mathcal{C}_3\mathcal{C}_4(b_2^{\diamond}a_5^{\diamond}\mathcal{S}_2\mathcal{C}_5-a_2^{\diamond}b_5^{\diamond}\mathcal{S}_5\mathcal{C}_2)\mathfrak{R}_{30}+ \tag{63}$$
$$+\mathcal{C}_1\mathcal{C}_2\mathcal{C}_4(b_3^{\diamond}a_5^{\diamond}\mathcal{S}_3\mathcal{C}_5-a_3^{\diamond}b_5^{\diamond}\mathcal{S}_5\mathcal{C}_3)\mathfrak{R}_{31}-\mathcal{C}_1\mathcal{C}_2\mathcal{C}_3(b_4^{\diamond}a_5^{\diamond}\mathcal{S}_4\mathcal{C}_5-a_4^{\diamond}b_5^{\diamond}\mathcal{S}_5\mathcal{C}_4)\mathfrak{R}_{32}\,.$$

where $\bar{\Delta}_i^{\diamond}$ = determinant of $A^{\diamond}$ when $i^{\text{th}}$ column of $A^{\diamond}$ is replaced by $\bar{B}$, which yield the following:

$$\bar{\Delta}_1^{\diamond}=\mathfrak{R}_{33}\tilde{\mathrm{F}}_3+\mathfrak{R}_{34}\tilde{\mathrm{F}}_4;\ \bar{\Delta}_2^{\diamond}=\mathfrak{R}_{35}\tilde{\mathrm{F}}_3+\mathfrak{R}_{36}\tilde{\mathrm{F}}_4;$$
$$\bar{\Delta}_3^{\diamond}=\mathfrak{R}_{37}\tilde{\mathrm{F}}_3+\mathfrak{R}_{38}\tilde{\mathrm{F}}_4;\ \bar{\Delta}_4^{\diamond}=\mathfrak{R}_{39}\tilde{\mathrm{F}}_3+\mathfrak{R}_{40}\tilde{\mathrm{F}}_4; \tag{64}$$
$$\bar{\Delta}_5^{\diamond}=\mathfrak{R}_{41}\tilde{\mathrm{F}}_3+\mathfrak{R}_{42}\tilde{\mathrm{F}}_4,$$

where

$$\mathfrak{R}_{29}=\bar{r}_1^{\diamond}\gamma_2^{\diamond}+\bar{r}_2^{\diamond}\gamma_3^{\diamond}+\bar{r}_3^{\diamond}\gamma_4^{\diamond}\,,$$

$\mathfrak{R}_{30} = \bar{r}_1^{\diamond}\gamma_1^{\diamond} + \bar{r}_4^{\diamond}\gamma_3^{\diamond} + \bar{r}_5^{\diamond}\gamma_4^{\diamond},$
$\mathfrak{R}_{31} = -\bar{r}_2^{\diamond}\gamma_1^{\diamond} + \bar{r}_4^{\diamond}\gamma_2^{\diamond} + \bar{r}_6^{\diamond}\gamma_4^{\diamond},$
$\mathfrak{R}_{32} = \bar{r}_3^{\diamond}\gamma_1^{\diamond} - \bar{r}_5^{\diamond}\gamma_2^{\diamond} + \bar{r}_6^{\diamond}\gamma_3^{\diamond},$
$\mathfrak{R}_{33} = (a_2^{\diamond}b_5^{\diamond}\mathcal{S}_5\mathcal{C}_2 - a_5^{\diamond}b_2^{\diamond}\mathcal{S}_2\mathcal{C}_5)\mathcal{C}_3\mathcal{C}_4\bar{\bar{r}}_1^{\diamond} + (a_3^{\diamond}b_5^{\diamond}\mathcal{S}_5\mathcal{C}_3 - a_5^{\diamond}b_3^{\diamond}\mathcal{S}_3\mathcal{C}_5)\mathcal{C}_2\mathcal{C}_4\bar{\bar{r}}_4^{\diamond} +$
$+(a_4^{\diamond}b_5^{\diamond}\mathcal{S}_5\mathcal{C}_4 - a_5^{\diamond}b_4^{\diamond}\mathcal{S}_4\mathcal{C}_5)\mathcal{C}_2\mathcal{C}_3\bar{\bar{r}}_6^{\diamond},$
$\mathfrak{R}_{34} = (a_2^{\diamond}b_5^{\diamond}\mathcal{S}_5\mathcal{C}_2 - a_5^{\diamond}b_2^{\diamond}\mathcal{S}_2\mathcal{C}_5)\mathcal{C}_3\mathcal{C}_4\bar{\bar{r}}_1^{\diamond} + (a_3^{\diamond}b_5^{\diamond}\mathcal{S}_5\mathcal{C}_3 - a_5^{\diamond}b_3^{\diamond}\mathcal{S}_3\mathcal{C}_5)\mathcal{C}_2\mathcal{C}_4\bar{\bar{r}}_2^{\diamond} +$
$+(a_4^{\diamond}b_5^{\diamond}\mathcal{S}_5\mathcal{C}_4 - a_5^{\diamond}b_4^{\diamond}\mathcal{S}_4\mathcal{C}_5)\mathcal{C}_2\mathcal{C}_3\bar{\bar{r}}_3^{\diamond},$
$\mathfrak{R}_{35} = (a_5^{\diamond}b_1^{\diamond}\mathcal{S}_1\mathcal{C}_5 - a_1^{\diamond}b_5^{\diamond}\mathcal{S}_5\mathcal{C}_1)\mathcal{C}_3\mathcal{C}_4\bar{\bar{r}}_1^{\diamond} + (a_5^{\diamond}b_3^{\diamond}\mathcal{S}_3\mathcal{C}_5 - a_3^{\diamond}b_5^{\diamond}\mathcal{S}_5\mathcal{C}_3)\mathcal{C}_1\mathcal{C}_4\bar{\bar{r}}_2^{\diamond} +$
$+(a_4^{\diamond}b_5^{\diamond}\mathcal{S}_5\mathcal{C}_4 - a_5^{\diamond}b_4^{\diamond}\mathcal{S}_4\mathcal{C}_5)\mathcal{C}_1\mathcal{C}_3\bar{\bar{r}}_3^{\diamond},$
$\mathfrak{R}_{36} = (a_5^{\diamond}b_1^{\diamond}\mathcal{S}_1\mathcal{C}_5 - a_1^{\diamond}b_5^{\diamond}\mathcal{S}_5\mathcal{C}_1)\mathcal{C}_3\mathcal{C}_4\bar{\bar{r}}_1^{\diamond} + (a_5^{\diamond}b_3^{\diamond}\mathcal{S}_3\mathcal{C}_5 - a_3^{\diamond}b_5^{\diamond}\mathcal{S}_5\mathcal{C}_3)\mathcal{C}_1\mathcal{C}_4\bar{\bar{r}}_4^{\diamond} +$
$+(a_5^{\diamond}b_4^{\diamond}\mathcal{S}_4\mathcal{C}_5 - a_4^{\diamond}b_5^{\diamond}\mathcal{S}_5\mathcal{C}_4)\mathcal{C}_1\mathcal{C}_3\bar{\bar{r}}_5^{\diamond},$
$\mathfrak{R}_{37} = (a_2^{\diamond}b_5^{\diamond}\mathcal{S}_5\mathcal{C}_2 - a_5^{\diamond}b_2^{\diamond}\mathcal{S}_2\mathcal{C}_5)\mathcal{C}_1\mathcal{C}_4\bar{\bar{r}}_2^{\diamond} + (a_5^{\diamond}b_1^{\diamond}\mathcal{S}_1\mathcal{C}_5 - a_1^{\diamond}b_5^{\diamond}\mathcal{S}_5\mathcal{C}_1)\mathcal{C}_2\mathcal{C}_4\bar{\bar{r}}_4^{\diamond} +$
$+(a_5^{\diamond}b_4^{\diamond}\mathcal{S}_4\mathcal{C}_5 - a_4^{\diamond}b_5^{\diamond}\mathcal{S}_5\mathcal{C}_4)\mathcal{C}_1\mathcal{C}_2\bar{\bar{r}}_5^{\diamond},$
$\mathfrak{R}_{38} = (a_5^{\diamond}b_1^{\diamond}\mathcal{S}_1\mathcal{C}_5 - a_1^{\diamond}b_5^{\diamond}\mathcal{S}_5\mathcal{C}_1)\mathcal{C}_2\mathcal{C}_4\bar{\bar{r}}_2^{\diamond} + (a_2^{\diamond}b_5^{\diamond}\mathcal{S}_5\mathcal{C}_2 - a_5^{\diamond}b_2^{\diamond}\mathcal{S}_2\mathcal{C}_5)\mathcal{C}_1\mathcal{C}_4\bar{\bar{r}}_4^{\diamond} +$
$+(a_4^{\diamond}b_5^{\diamond}\mathcal{S}_5\mathcal{C}_4 - a_5^{\diamond}b_4^{\diamond}\mathcal{S}_4\mathcal{C}_5)\mathcal{C}_1\mathcal{C}_2\bar{\bar{r}}_6^{\diamond},$
$\mathfrak{R}_{39} = (a_5^{\diamond}b_2^{\diamond}\mathcal{S}_2\mathcal{C}_5 - a_2^{\diamond}b_5^{\diamond}\mathcal{S}_5\mathcal{C}_2)\mathcal{C}_1\mathcal{C}_3\bar{\bar{r}}_3^{\diamond} + (a_3^{\diamond}b_5^{\diamond}\mathcal{S}_5\mathcal{C}_3 - a_5^{\diamond}b_3^{\diamond}\mathcal{S}_3\mathcal{C}_5)\mathcal{C}_1\mathcal{C}_2\bar{\bar{r}}_5^{\diamond} +$
$+(a_5^{\diamond}b_1^{\diamond}\mathcal{S}_1\mathcal{C}_5 - a_1^{\diamond}b_5^{\diamond}\mathcal{S}_5\mathcal{C}_1)\mathcal{C}_2\mathcal{C}_3\bar{\bar{r}}_6^{\diamond},$
$\mathfrak{R}_{40} = (a_5^{\diamond}b_1^{\diamond}\mathcal{S}_1\mathcal{C}_5 - a_1^{\diamond}b_5^{\diamond}\mathcal{S}_5\mathcal{C}_1)\mathcal{C}_2\mathcal{C}_3\bar{\bar{r}}_3^{\diamond} + (a_2^{\diamond}b_5^{\diamond}\mathcal{S}_5\mathcal{C}_2 - a_5^{\diamond}b_2^{\diamond}\mathcal{S}_2\mathcal{C}_5)\mathcal{C}_1\mathcal{C}_3\bar{\bar{r}}_5^{\diamond} +$
$+(a_5^{\diamond}b_3^{\diamond}\mathcal{S}_3\mathcal{C}_5 - a_3^{\diamond}b_5^{\diamond}\mathcal{S}_5\mathcal{C}_3)\mathcal{C}_1\mathcal{C}_2\bar{\bar{r}}_6^{\diamond},$
$\mathfrak{R}_{41} = -b_1^{\diamond}\mathcal{S}_1\mathcal{C}_2\mathcal{C}_3\mathcal{C}_4(a_2^{\diamond}\bar{\bar{r}}_1^{\diamond} + a_3^{\diamond}\bar{\bar{r}}_4^{\diamond} + a_4^{\diamond}\bar{\bar{r}}_6^{\diamond}) + b_2^{\diamond}\mathcal{S}_2\mathcal{C}_1\mathcal{C}_3\mathcal{C}_4(a_1^{\diamond}\bar{\bar{r}}_1^{\diamond} + a_3^{\diamond}\bar{\bar{r}}_2^{\diamond} - a_4^{\diamond}\bar{\bar{r}}_3^{\diamond}) +$
$+b_3^{\diamond}\mathcal{S}_3\mathcal{C}_1\mathcal{C}_2\mathcal{C}_4(a_1^{\diamond}\bar{\bar{r}}_4^{\diamond} - a_2^{\diamond}\bar{\bar{r}}_2^{\diamond} + a_4^{\diamond}\bar{\bar{r}}_5^{\diamond}) + b_4^{\diamond}\mathcal{S}_4\mathcal{C}_1\mathcal{C}_2\mathcal{C}_3(a_1^{\diamond}\bar{\bar{r}}_6^{\diamond} + a_2^{\diamond}\bar{\bar{r}}_3^{\diamond} - a_3^{\diamond}\bar{\bar{r}}_5^{\diamond}),$
$\mathfrak{R}_{42} = b_1^{\diamond}\mathcal{S}_1\mathcal{C}_2\mathcal{C}_3\mathcal{C}_4(a_2^{\diamond}\bar{r}_1^{\diamond} + a_3^{\diamond}\bar{r}_2^{\diamond} + a_4^{\diamond}\bar{r}_3^{\diamond}) - b_2^{\diamond}\mathcal{S}_2\mathcal{C}_1\mathcal{C}_3\mathcal{C}_4(a_1^{\diamond}\bar{r}_1^{\diamond} + a_3^{\diamond}\bar{r}_4^{\diamond} + a_4^{\diamond}\bar{r}_5^{\diamond}) +$
$+b_3^{\diamond}\mathcal{S}_3\mathcal{C}_1\mathcal{C}_2\mathcal{C}_4(-a_1^{\diamond}\bar{r}_2^{\diamond} + a_2^{\diamond}\bar{r}_4^{\diamond} + a_4^{\diamond}\bar{r}_6^{\diamond}) - b_4^{\diamond}\mathcal{S}_4\mathcal{C}_1\mathcal{C}_2\mathcal{C}_3(a_1^{\diamond}\bar{r}_3^{\diamond} - a_2^{\diamond}\bar{r}_5^{\diamond} + a_3^{\diamond}\bar{r}_6^{\diamond}),$

where

$\bar{r}_1^{\diamond} = \alpha_3^{\diamond}\beta_4^{\diamond} - \alpha_4^{\diamond}\beta_3^{\diamond},\ \bar{r}_2^{\diamond} = \alpha_4^{\diamond}\beta_2^{\diamond} - \alpha_2^{\diamond}\beta_4^{\diamond},\ \bar{r}_3^{\diamond} = \alpha_2^{\diamond}\beta_3^{\diamond} - \alpha_3^{\diamond}\beta_2^{\diamond},$
$\bar{r}_4^{\diamond} = \alpha_4^{\diamond}\beta_1^{\diamond} - \alpha_1^{\diamond}\beta_4^{\diamond},\ \bar{r}_5^{\diamond} = \alpha_1^{\diamond}\beta_3^{\diamond} - \alpha_3^{\diamond}\beta_1^{\diamond},\ \bar{r}_6^{\diamond} = \alpha_1^{\diamond}\beta_2^{\diamond} - \alpha_2^{\diamond}\beta_1^{\diamond},$
$\bar{\bar{r}}_1^{\diamond} = \alpha_4^{\diamond}\gamma_3^{\diamond} - \alpha_3^{\diamond}\gamma_4^{\diamond},\ \bar{\bar{r}}_2^{\diamond} = \alpha_1^{\diamond}\gamma_4^{\diamond} - \alpha_4^{\diamond}\gamma_1^{\diamond},\ \bar{\bar{r}}_3^{\diamond} = \alpha_1^{\diamond}\gamma_3^{\diamond} - \alpha_3^{\diamond}\gamma_1^{\diamond},$
$\bar{\bar{r}}_4^{\diamond} = \alpha_2^{\diamond}\gamma_4^{\diamond} - \alpha_4^{\diamond}\gamma_2^{\diamond},\ \bar{\bar{r}}_5^{\diamond} = \alpha_1^{\diamond}\gamma_2^{\diamond} - \alpha_2^{\diamond}\gamma_1^{\diamond},\ \bar{\bar{r}}_6^{\diamond} = \alpha_3^{\diamond}\gamma_2^{\diamond} - \alpha_2^{\diamond}\gamma_3^{\diamond}.$

Inserting the values of $\bar{C}_i^{\diamond}$ from Eq. (63) in Eqs. (40), (45)–(47), and (49) ascertain the displacement components, temperature distribution, carrier density distribution, moisture, and stress components as:

$\tilde{u}_1 = \frac{1}{\bar{\Delta}_i^{\diamond}}\left(\mathfrak{S}_{15}^{\diamond}\tilde{\mathrm{F}}_3 + \mathfrak{S}_{16}^{\diamond}\tilde{\mathrm{F}}_4\right),\ \tilde{u}_3 = \frac{1}{\bar{\Delta}_i^{\diamond}}\left(\mathfrak{S}_{17}^{\diamond}\tilde{\mathrm{F}}_3 + \mathfrak{S}_{18}^{\diamond}\tilde{\mathrm{F}}_4\right),\ \tilde{T} = \frac{1}{\bar{\Delta}_i^{\diamond}}\left(\mathfrak{S}_{19}^{\diamond}\tilde{\mathrm{F}}_3 + \mathfrak{S}_{20}^{\diamond}\tilde{\mathrm{F}}_4\right),$
$\tilde{N} = \frac{1}{\bar{\Delta}_i^{\diamond}}\left(\mathfrak{S}_{21}^{\diamond}\tilde{\mathrm{F}}_3 + \mathfrak{S}_{22}^{\diamond}\tilde{\mathrm{F}}_4\right),\ \tilde{M} = \frac{1}{\bar{\Delta}_i^{\diamond}}\left(\mathfrak{S}_{23}^{\diamond}\tilde{\mathrm{F}}_3 + \mathfrak{S}_{24}^{\diamond}\tilde{\mathrm{F}}_4\right),\ \tilde{t}_{33} = \frac{1}{\bar{\Delta}_i^{\diamond}}\left(\mathfrak{S}_{25}^{\diamond}\tilde{\mathrm{F}}_3 + \mathfrak{S}_{26}^{\diamond}\tilde{\mathrm{F}}_4\right),$
$\tilde{t}_{31} = \frac{1}{\bar{\Delta}_i^{\diamond}}\left(\mathfrak{S}_{27}^{\diamond}\tilde{\mathrm{F}}_3 + \mathfrak{S}_{28}^{\diamond}\tilde{\mathrm{F}}_4\right),$

where

$\mathfrak{S}_{15}^{\diamond} = -\mathrm{i}\xi\sum_{i=0}^{3}\bar{\mathfrak{R}}_{2i+1}^{\diamond} - m_5^{\diamond}\bar{\mathfrak{R}}_9^{\diamond},\ \mathfrak{S}_{16}^{\diamond} = -\mathrm{i}\xi\sum_{i=1}^{4}\bar{\mathfrak{R}}_{2i}^{\diamond} - m_5^{\diamond}\bar{\mathfrak{R}}_{10}^{\diamond},$
$\mathfrak{S}_{17}^{\diamond} = \sum_{i=5}^{8}m_{i-4}^{\diamond}\bar{\mathfrak{R}}_{2i+1}^{\diamond} - \mathrm{i}\xi\bar{\mathfrak{R}}_{19}^{\diamond},\ \mathfrak{S}_{18}^{\diamond} = \sum_{i=5}^{8}m_{i-4}^{\diamond}\bar{\mathfrak{R}}_{2i+2}^{\diamond} - \mathrm{i}\xi\bar{\mathfrak{R}}_{20}^{\diamond},\ \mathfrak{S}_{19}^{\diamond} = \sum_{i=0}^{3}\alpha_{i+1}^{\diamond}\bar{\mathfrak{R}}_{2i+1}^{\diamond},$
$\mathfrak{S}_{20}^{\diamond} = \sum_{i=0}^{3}\alpha_{i+1}^{\diamond}\bar{\mathfrak{R}}_{2i+2}^{\diamond},\ \mathfrak{S}_{21}^{\diamond} = \sum_{i=0}^{3}\beta_{i+1}^{\diamond}\bar{\mathfrak{R}}_{2i+1}^{\diamond},\ \mathfrak{S}_{22}^{\diamond} = \sum_{i=0}^{3}\beta_{i+1}^{\diamond}\bar{\mathfrak{R}}_{2i+2}^{\diamond},$
$\mathfrak{S}_{23}^{\diamond} = \sum_{i=0}^{3}\gamma_{i+1}^{\diamond}\bar{\mathfrak{R}}_{2i+1}^{\diamond},\ \mathfrak{S}_{24}^{\diamond} = \sum_{i=0}^{3}\gamma_{i+1}^{\diamond}\bar{\mathfrak{R}}_{2i+2}^{\diamond},\ \mathfrak{S}_{25}^{\diamond} = \sum_{i=0}^{4}a_{i+1}^{\diamond}\bar{\mathfrak{R}}_{2i+1}^{\diamond},$
$\mathfrak{S}_{26}^{\diamond} = \sum_{i=0}^{4}b_{i+1}^{\diamond}\bar{\mathfrak{R}}_{2i+2}^{\diamond},\ \mathfrak{S}_{27}^{\diamond} = \sum_{i=5}^{9}b_{i-4}^{\diamond}\bar{\mathfrak{R}}_{2i+1}^{\diamond},\ \mathfrak{S}_{28}^{\diamond} = \sum_{i=5}^{9}b_{i-4}^{\diamond}\bar{\mathfrak{R}}_{2i+2}^{\diamond},$

where

$\bar{\mathfrak{R}}_1^{\diamond} = \mathfrak{R}_{33}\mathcal{C}_1, \bar{\mathfrak{R}}_2^{\diamond} = \mathfrak{R}_{34}\mathcal{C}_1, \bar{\mathfrak{R}}_3^{\diamond} = \mathfrak{R}_{35}\mathcal{C}_2, \bar{\mathfrak{R}}_4^{\diamond} = \mathfrak{R}_{36}\mathcal{C}_2, \bar{\mathfrak{R}}_5^{\diamond} = \mathfrak{R}_{37}\mathcal{C}_3, \bar{\mathfrak{R}}_6^{\diamond} = \mathfrak{R}_{38}\mathcal{C}_3,$
$\bar{\mathfrak{R}}_7^{\diamond} = \mathfrak{R}_{39}\mathcal{C}_4, \bar{\mathfrak{R}}_8^{\diamond} = \mathfrak{R}_{40}\mathcal{C}_4, \bar{\mathfrak{R}}_9^{\diamond} = \mathfrak{R}_{41}\mathcal{C}_5, \bar{\mathfrak{R}}_{10}^{\diamond} = \mathfrak{R}_{42}\mathcal{C}_5, \bar{\mathfrak{R}}_{11}^{\diamond} = \mathfrak{R}_{33}\mathcal{S}_1, \bar{\mathfrak{R}}_{12}^{\diamond} = \mathfrak{R}_{34}\mathcal{S}_1,$
$\bar{\mathfrak{R}}_{13}^{\diamond} = \mathfrak{R}_{35}\mathcal{S}_1, \bar{\mathfrak{R}}_{14}^{\diamond} = \mathfrak{R}_{36}\mathcal{S}_1, \bar{\mathfrak{R}}_{15}^{\diamond} = \mathfrak{R}_{37}\mathcal{S}_1, \bar{\mathfrak{R}}_{16}^{\diamond} = \mathfrak{R}_{38}\mathcal{S}_1, \bar{\mathfrak{R}}_{17}^{\diamond} = \mathfrak{R}_{39}\mathcal{S}_1, \bar{\mathfrak{R}}_{18}^{\diamond} = \mathfrak{R}_{40}\mathcal{S}_1,$

$\overline{\mathrm{R}}_{19}^{\diamond} = \Re_{41}\mathcal{S}_1, \overline{\mathrm{R}}_{20}^{\diamond} = \Re_{42}\mathcal{S}_1.$

**Particular cases**

*Case 1:* For carrier density source $\mathrm{F}_{40} = 0$ yield:

$$\left(\tilde{u}_1, \tilde{u}_3, \tilde{T}, \tilde{N}, \tilde{M}, \tilde{t}_{33}, \tilde{t}_{31}\right) = \frac{1}{\Delta_i^{\diamond}}\left(\mathfrak{S}_{15}^{\diamond}, \mathfrak{S}_{17}^{\diamond}, \mathfrak{S}_{19}^{\diamond}, \mathfrak{S}_{21}^{\diamond}, \mathfrak{S}_{23}^{\diamond}, \mathfrak{S}_{25}^{\diamond}, \mathfrak{S}_{27}^{\diamond}\right)\tilde{\mathrm{F}}_3. \tag{66}$$

*Case 2:* For moisture source $\mathrm{F}_{30} = 0$ yield:

$$\left(\tilde{u}_1, \tilde{u}_3, \tilde{T}, \tilde{N}, \tilde{M}, \tilde{t}_{33}, \tilde{t}_{31}\right) = \frac{1}{\Delta_i^{\diamond}}\left(\mathfrak{S}_{16}^{\diamond}, \mathfrak{S}_{18}^{\diamond}, \mathfrak{S}_{20}^{\diamond}, \mathfrak{S}_{22}^{\diamond}, \mathfrak{S}_{24}^{\diamond}, \mathfrak{S}_{26}^{\diamond}, \mathfrak{S}_{28}^{\diamond}\right)\tilde{\mathrm{F}}_4. \tag{67}$$

**Special case**

In absence of moisture impact i.e. when $D_t^m = 0, K_m = 0, \gamma_m = 0$ yield the corresponding results for isotropic photothermoelastic plate, then Eq. (39) takes the form:

$$\left(D^6 + \mathfrak{B}_{p1}D^4 + \mathfrak{B}_{p2}D^2 + \mathfrak{B}_{p3}\right)\left(\widetilde{\Phi}, \tilde{T}, \widetilde{N}\right) = 0, \tag{68}$$

where

$\mathfrak{B}_{p1} = \Re_{p1} - \Re_{p3} - \xi^2 - \mathfrak{s}^2$; $\mathfrak{B}_{p2} = \Re_{p2} - \xi^2\Re_{p1} - \mathfrak{s}^2\Re_{p1} - \Re_{p4} - \Re_{p6}$,

$\mathfrak{B}_{p3} = -\xi^2\Re_{p2} - \mathfrak{s}^2\Re_{p2} - \Re_{p5} - \Re_{p7}$,

where

$\Re_{p1} = -2\xi^2 - f_{13}\,\mathfrak{s} - f_{14} - \mathcal{r}_1 f_{17}$ ,

$\Re_{p2} = \xi^4 + f_{13}\mathfrak{s}\xi^2 + f_{14}\xi^2 + f_{17}\mathcal{r}_1\xi^2 + f_{13}f_{17}\mathcal{r}_1\mathfrak{s} + f_{14}f_{17}\mathcal{r}_1 - f_{15}f_{16}$ ,

$\Re_{p3} = f_{18}\mathcal{r}_1$ ; $\Re_{p4} = -2f_{18}\mathcal{r}_1\xi^2 - f_{13}f_{18}\mathcal{r}_1\mathfrak{s} - f_{14}f_{18}\mathcal{r}_1$,

$\Re_{p5} = f_{18}\mathcal{r}_1\xi^4 + f_{13}f_{18}\mathcal{r}_1\mathfrak{s}\xi^2 + f_{14}f_{18}\mathcal{r}_1\xi^2$,

$\Re_{p6} = -f_{15}f_{18}\mathcal{r}_1$ , $\Re_{p7} = f_{15}f_{18}\mathcal{r}_1\xi^2$.

The general solution of Eq. (68) is represented as:

$$\left(\widetilde{\Phi}, \tilde{T}, \widetilde{N}\right) = \sum_{i=1}^{3}\left(1, \alpha_{pi}, \beta_{pi}\right)\bar{C}_{pi}\cosh m_{pi}\,x_3, \tag{69}$$

where $m_{pi}(i = 1, 2, 3)$ are roots of $D^6 + \mathfrak{B}_{p1}D^4 + \mathfrak{B}_{p2}D^2 + \mathfrak{B}_{p3} = 0$.

The coupling parameters $\alpha_{pi}, \beta_{pi}$ are given by:

$$\alpha_{pi} = \sum_{i=1}^{3}\frac{\Re_{p3}m_{pi}^4 + \Re_{p4}m_{pi}^2 + \Re_{p5}}{m_{pi}^4 + \Re_{p1}m_{pi}^2 + \Re_{p2}}, \tag{70}$$

$$\beta_{pi} = \sum_{i=1}^{3}\frac{\Re_{p6}m_{pi}^2 + \Re_{p7}}{m_{pi}^4 + \Re_{p1}m_{pi}^2 + \Re_{p2}}\ . \tag{71}$$

In this case, $\widetilde{\Psi} = \bar{C}_{p4}\sinh m_{p4}x_3$, where $m_{p4}$ is a root of equation $D^2 + \mathfrak{B}_{p4} = 0$ , $\mathfrak{B}_{p4}$ is same as $\mathfrak{B}_6$ and $m_{p4}$ is same as $m_5^{\diamond}$.

Transformed boundary restrictions in this case lead to:

$$\tilde{t}_{33} = 0,\ \ \tilde{t}_{31} = 0,\ \ \tilde{T} = 0,\ \ \widetilde{N} = \tilde{\mathrm{F}}_3(\xi, x_3, \mathfrak{s}) \text{ at } x_3 = \pm d. \tag{72}$$

Utilizing these revised boundary restrictions, we compute the associated results as

$$\begin{aligned}
&\tilde{u}_1 = \frac{1}{\Delta_p}\left(\overline{\mathfrak{S}}_{p1}\tilde{\mathrm{F}}_3\right),\ \ \tilde{u}_3 = \frac{1}{\Delta_p}\left(\overline{\mathfrak{S}}_{p2}\tilde{\mathrm{F}}_3\right),\\
&\tilde{T} = \frac{1}{\Delta_p}\left(\overline{\mathfrak{S}}_{p3}\tilde{\mathrm{F}}_3\right),\ \ \widetilde{N} = \frac{1}{\Delta_p}\left(\overline{\mathfrak{S}}_{p4}\tilde{\mathrm{F}}_3\right),\\
&\tilde{t}_{33} = \frac{1}{\Delta_p}\left(\overline{\mathfrak{S}}_{p5}\tilde{\mathrm{F}}_3\right),\ \ \tilde{t}_{31} = \frac{1}{\Delta_p}\left(\overline{\mathfrak{S}}_{p6}\tilde{\mathrm{F}}_3\right),
\end{aligned} \tag{73}$$

where

$\Delta_p$ is determinant of matrix $A_p$ which is given by:

$$A_p = \begin{bmatrix} a_{p1}\mathcal{C}_{p1} & a_{p2}\mathcal{C}_{p2} & a_{p3}\mathcal{C}_{p3} & a_{p4}\mathcal{C}_{p4} \\ b_{p1}\mathcal{S}_{p1} & b_{p2}\mathcal{S}_{p2} & b_{p3}\mathcal{S}_{p3} & b_{p4}\mathcal{S}_{p4} \\ \alpha_{p1}\mathcal{C}_{p1} & \alpha_{p2}\mathcal{C}_{p2} & \alpha_{p3}\mathcal{C}_{p3} & 0 \\ \beta_{p1}\mathcal{C}_{p1} & \beta_{p2}\mathcal{C}_{p2} & \beta_{p3}\mathcal{C}_{p3} & 0 \end{bmatrix},$$

with

$\overline{\mathcal{S}}_{p1} = -\mathrm{i}\xi \sum_{i=1}^{3} \overline{\mathrm{R}}_i^p - m_{p4}\mathrm{R}_4^p,\ \overline{\mathcal{S}}_{p2} = \sum_{i=1}^{3} m_{pi}\overline{\mathrm{R}}_{i+4}^p - \mathrm{i}\xi \mathrm{R}_8^p,\ \overline{\mathcal{S}}_{p3} = \sum_{i=1}^{3} \alpha_{pi}\overline{\mathrm{R}}_i^p,$
$\overline{\mathcal{S}}_{p4} = \sum_{i=1}^{3} \beta_{pi}\overline{\mathrm{R}}_i^p,\ \overline{\mathcal{S}}_{p5} = \sum_{i=1}^{4} a_{pi}\overline{\mathrm{R}}_i^p, \overline{\mathcal{S}}_{p6} = \sum_{i=1}^{4} b_{pi}\overline{\mathrm{R}}_{i+4}^p,$

and

$\overline{\mathrm{R}}_1^p = \overline{\mathfrak{R}}_{p8}\mathcal{C}_{p1},\ \overline{\mathrm{R}}_2^p = \overline{\mathfrak{R}}_{p9}\mathcal{C}_{p2}, \overline{\mathrm{R}}_3^p = \overline{\mathfrak{R}}_{p10}\mathcal{C}_{p3},\ \overline{\mathrm{R}}_4^p = \overline{\mathfrak{R}}_{p11}\mathcal{C}_{p4},$
$\overline{\mathrm{R}}_5^p = \overline{\mathfrak{R}}_{p8}\mathcal{S}_{p1},\ \overline{\mathrm{R}}_6^p = \overline{\mathfrak{R}}_{p9}\mathcal{S}_{p2},\ \overline{\mathrm{R}}_7^p = \overline{\mathfrak{R}}_{p10}\mathcal{S}_{p3},\ \overline{\mathrm{R}}_8^p = \overline{\mathfrak{R}}_{p11}\mathcal{S}_{p4},$

where

$\overline{\mathfrak{R}}_{p8} = a_{p2}b_{p4}\alpha_{p3}\mathcal{C}_{p2}\mathcal{C}_{p3}\mathcal{S}_{p4} - a_{p3}b_{p4}\alpha_{p2}\mathcal{C}_{p2}\mathcal{C}_{p3}\mathcal{S}_{p4} +$
$+a_{p3}\mathcal{C}_{p4}\left(b_{p3}\alpha_{p2}\mathcal{C}_{p2}\mathcal{S}_{p3} - b_{p2}\alpha_{p3}\mathcal{C}_{p3}\mathcal{S}_{p2}\right),$
$\overline{\mathfrak{R}}_{p9} = -a_{p1}b_{p4}\alpha_{p3}\mathcal{C}_{p1}\mathcal{C}_{p3}\mathcal{S}_{p4} + a_{p3}b_{p4}\alpha_{p1}\mathcal{C}_{p1}\mathcal{C}_{p3}\mathcal{S}_{p4} +$
$+a_{p4}\mathcal{C}_{p4}\left(b_{p1}\alpha_{p3}\mathcal{C}_{p3}\mathcal{S}_{p1} - b_{p3}\alpha_{p1}\mathcal{C}_{p1}\mathcal{S}_{p3}\right),$
$\overline{\mathfrak{R}}_{p10} = a_{p1}b_{p4}\alpha_{p2}\mathcal{C}_{p1}\mathcal{C}_{p2}\mathcal{S}_{p4} - a_{p2}b_{p4}\alpha_{p1}\mathcal{C}_{p1}\mathcal{C}_{p2}\mathcal{S}_{p4} +$
$+a_{p4}\mathcal{C}_{p4}\left(b_{p2}\alpha_{p1}\mathcal{C}_{p1}\mathcal{S}_{p2} - b_{p1}\alpha_{p2}\mathcal{C}_{p2}\mathcal{S}_{p1}\right),$
$\overline{\mathfrak{R}}_{p11} = a_{p1}\mathcal{C}_{p1}\left(b_{p2}\alpha_{p3}\mathcal{C}_{p3}\mathcal{S}_{p2} - b_{p3}\alpha_{p2}\mathcal{C}_{p2}\mathcal{S}_{p3}\right) +$
$-a_{p2}\mathcal{C}_{p2}\left(b_{p1}\alpha_{p3}\mathcal{C}_{p3}\mathcal{S}_{p1} - b_{p3}\alpha_{p1}\mathcal{C}_{p1}\mathcal{S}_{p3}\right) + a_{p3}\mathcal{C}_{p3}\left(b_{p1}\alpha_{p2}\mathcal{C}_{p2}\mathcal{S}_{p1} - b_{p2}\alpha_{p1}\mathcal{C}_{p1}\mathcal{S}_{p2}\right).$

## Numerical outcomes and interpretation

For the mathematical calculations, we implement the isotropic Silicon (Si) material constants (Alenazi et al. [49], Table 1).

**Table 1.** Material constants for the isotropic Silicon (Si) material

| Symbol, Unit | Value | Symbol, Unit | Value |
|---|---|---|---|
| $\lambda, \mathrm{N/m^2}$ | $6.4 \cdot 10^{10}$ | $E_g, \mathrm{eV}$ | 1.11 |
| $\mu, \mathrm{N/m^2}$ | $6.5 \cdot 10^{10}$ | $D_t^m, \mathrm{m^2(\%H_2O)/s(K)}$ | $2.1 \cdot 10^{-7}$ |
| $\alpha_t, \mathrm{K^{-1}}$ | $4.14 \cdot 10^{-6}$ | $T_o, \mathrm{K}$ | 800 |
| $\alpha_n, \mathrm{m^3}$ | $-9 \cdot 10^{-31}$ | $K_m, \mathrm{(kg/msM)}$ | $2.2 \cdot 10^{-8}$ |
| $\alpha_m, \mathrm{cm/cm(\%H_2O)}$ | $2.68 \cdot 10^{-3}$ | $D_m, \mathrm{m^2\ s^{-1}}$ | $0.35 \cdot 10^{-2}$ |
| $\rho, \mathrm{kg/m^3}$ | 2330 | $D_m^t, \mathrm{m^2s(K)/(\%H_2O)}$ | $0.648 \cdot 10^{-6}$ |
| $D_\mathrm{e}, \mathrm{m^2/s}$ | $2.5 \cdot 10^{-3}$ | $k, \mathrm{Wm^{-1}K^{-1}}$ | 150 |
| $\tau, \mathrm{s}$ | $5 \cdot 10^{-5}$ | $n_o, \mathrm{m^{-3}}$ | $10^{10}$ |
| $\delta, \mathrm{m^{-3}\ K^{-1}}$ | 0.5 | $m_o$ | 10 % |
| $C_\mathrm{e}, \mathrm{J/(kgK)}$ | 695 | | |

The Matlab (R2014a) software is utilized for computing in the following scenarios:
Photothermoelastic moisture plate with $\tau_o = .03, \tau^o = .02$ (IPTMT1);
Photothermoelastic moisture plate with $\tau_o = .05, \tau^o = .04$ (IPTMT2);
Photothermoelastic moisture plate with $\tau_o = .03, \tau^o = .04$ (IPTMT3);
Photothermoelastic moisture plate with $\tau_o = 0, \tau^o = 0$ (IPTMT4);
Photothermoelastic without moisture plate $\tau_o = .03, \tau^o = 0$ (IPTWMT1);
Photothermoelastic without moisture plate $\tau_o = .05, \tau^o = 0$ (IPTWMT2).

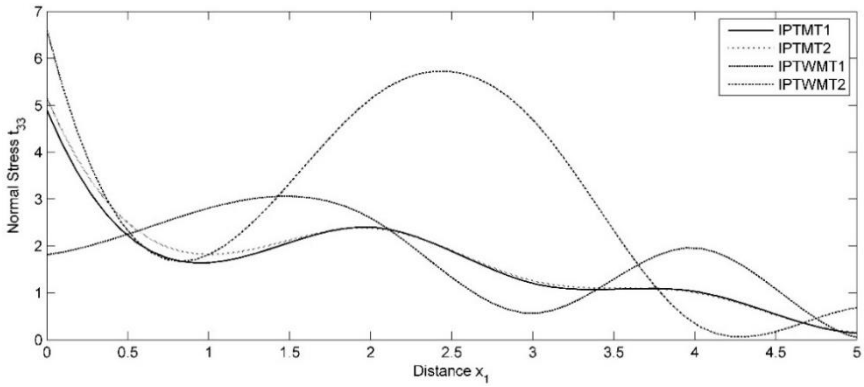


**Fig. 1.** Variation of normal stress $t_{33}$ w.r.t. $x_1$ owing to carrier density source

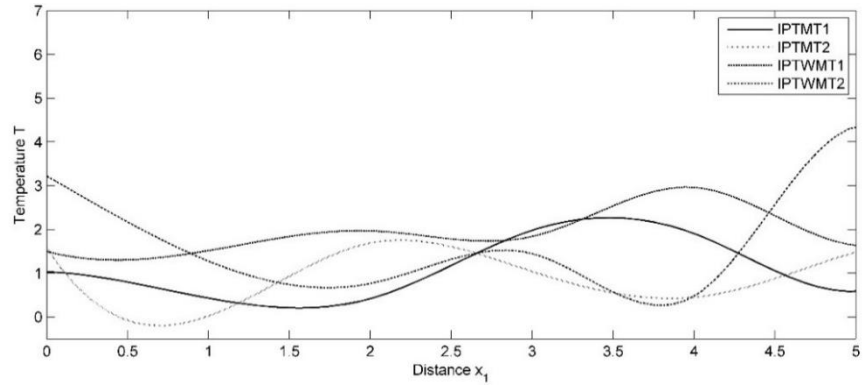


**Fig. 2.** Variation of temperature *T* w.r.t. $x_1$ owing to carrier density source

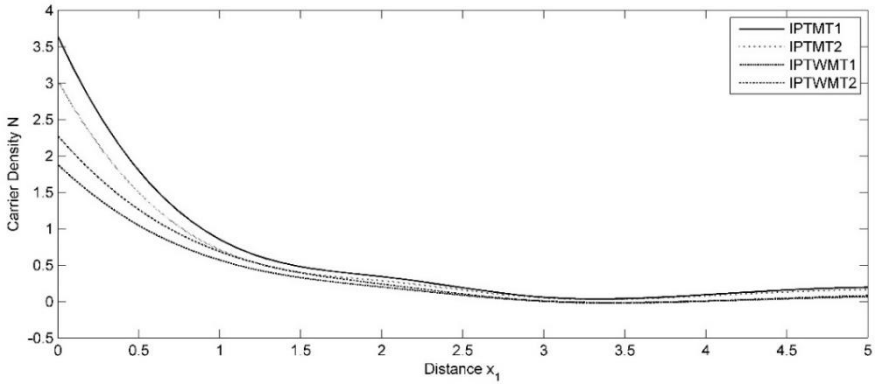


**Fig. 3.** Variation of carrier density *N* w.r.t. $x_1$ owing to carrier density source

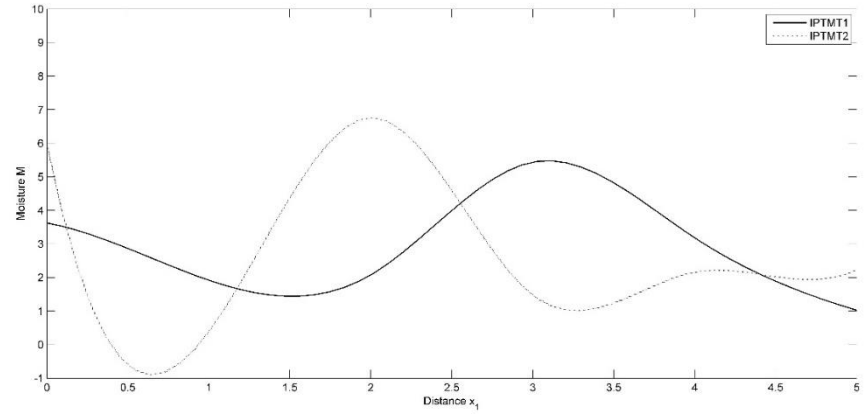


**Fig. 4.** Variation of moisture *M* w.r.t. $x_1$ owing to carrier density source

Figures 1–4 represent how moisture affects the field variables $(t_{33}, T, N, M)$ when there is carrier density source. Figures 5–8 represent the impact of relaxation times in case of carrier density source and Figures 9–12 represent the impact of relaxation times in case of moisture source on the same field variables $(t_{33}, T, N, M)$.

In all the figures, the solid line (——— ) represents IPTMT1, the dotted (⋯⋯⋯) line represents IPTMT2, the solid line containing the center symbol square (— ▫ —) indicates to IPTMT3 and the solid line containing the center symbol triangle (— △ —) represents IPTMT4, the dash (— — —) line corresponds to IPTWMT1, the dash dot (— · — · —) line corresponds to IPTWMT2.

Figure 1 displays the variation of normal stress $t_{33}$ with $x_1$. With the exception of the IPTMT1 model, $t_{33}$ for the IPTMT2, IPTWMT1, and IPTWMT2 models exhibit a declining trend in proximity to the source. Across the entire domain, $t_{33}$ reflects identical behavior with less fluctuations for the IPTMT1 and IPTMT2 models whereas it fluctuates more and displays an opposing oscillatory pattern for the IPTWMT1 and IPTWMT2 models.

Figure 2 presents the variation of temperature *T* with $x_1$. *T* exhibits a large-scale oscillating behavior for the IPTWMT2 model. T for IPTWMT1 and IPTWMT2 demonstrates a decreasing tendency initially, and it tracks the opposite trend for $0.5 \leq x_1$. T for IPTMT1 and IPTMT2 displays an overall opposing oscillating pattern, with the exception of some limited region where their behavior aligns.

Figure 3 shows how the carrier density *N* changes with $x_1$. Close to the source, all models exhibits a decreasing trend in *N*, with the IPTMT1 model showing the steepest decline. *N* for all models possess a pattern of minor oscillations within the range $1.5 \leq x_1 \leq 3$, followed by a slight and monotonic increasing trend thereafter.

Figure 4 depicts the variation of moisture *M* with $x_1$. In the range $0 \leq x_1 \leq 3$, *M* for IPTMT2 exhibits more pronounced oscillatory trend, followed by slight oscillations thereafter. *M* for IPTMT2 decreases within the range $0 \leq x_1 \leq 1.5$, transitioning into oscillatory behavior beyond this interval.

Figure 5 demonstrates the variation of normal stress $t_{33}$ with $x_1$. All models indicate a declining pattern in $t_{33}$ near the source, with the IPTMT3 model showing the highest magnitude and the IPTMT4 model depicting the smallest magnitude. As $x_1$ increases $t_{33}$ continues to decline with minor oscillations with slight variations in magnitude across the models.

Figure 6 illustrates how temperature *T* varies with $x_1$. With the exception of a limited initial segment, *T* for IPTMT1 and IPTMT2 reflect the opposite oscillatory patterns. *T* for the IPTMT3 and IPTMT4 models exhibit an opposite fluctuating behavior within the range $0 \leq x_1 \leq 3$ but beyond this interval their trends aligns.

Figure 7 depicts the variation of carrier density *N* with $x_1$. Close to the source, all models reveal a decreasing trend in *N*, with IPTMT3, reaching the highest magnitude and IPTMT2 the lowest. As the distance increases, *N* begins to oscillate slightly, tends to converge, and shows an increasing trend across all models.

Figure 8 shows how moisture *M* changes along $x_1$. *M* for IPTMT1 and IPTMT2 exhibit opposite oscillatory patterns throughout the entire domain, except for an initial small region where their responses temporarily align. On the other hand, *M* for IPTMT3 and IPTMT4 display inverse oscillatory behaviors within the range $0 \leq x_1 \leq 2.25$, subsequently exhibiting comparable behavior thereafter.

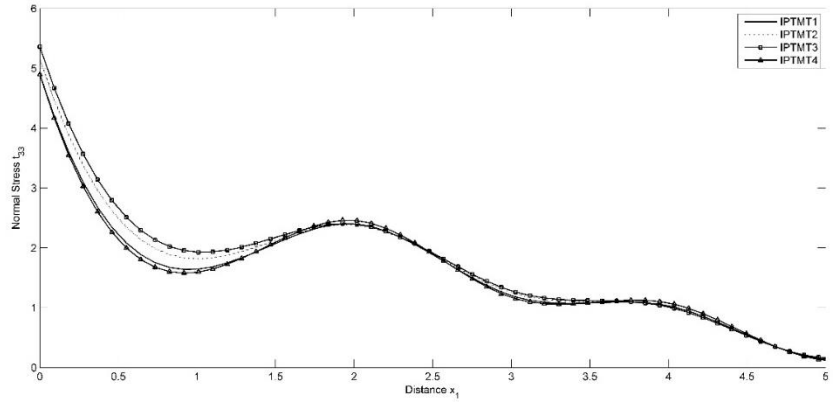


**Fig. 5.** Impact of relaxation times on normal stress $t_{33}$ due to carrier density source

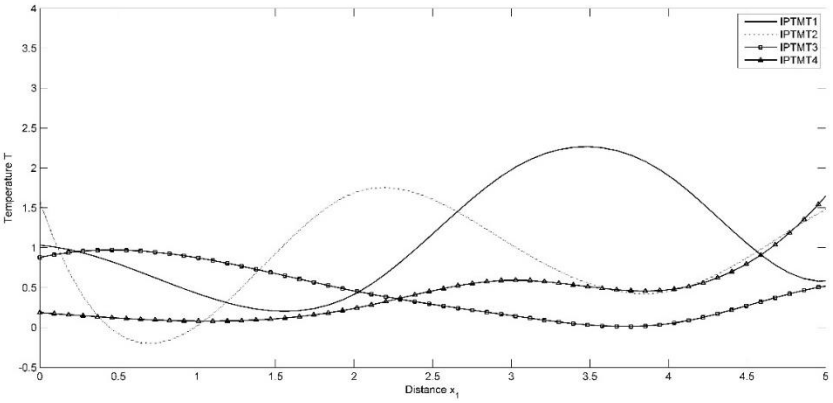


**Fig. 6.** Impact of relaxation times on temperature *T* due to carrier density source

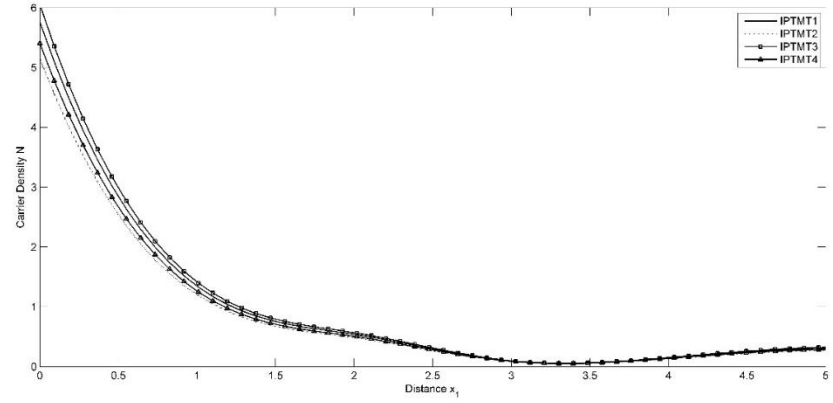


**Fig. 7.** Impact of relaxation times on carrier density *N* due to carrier density source

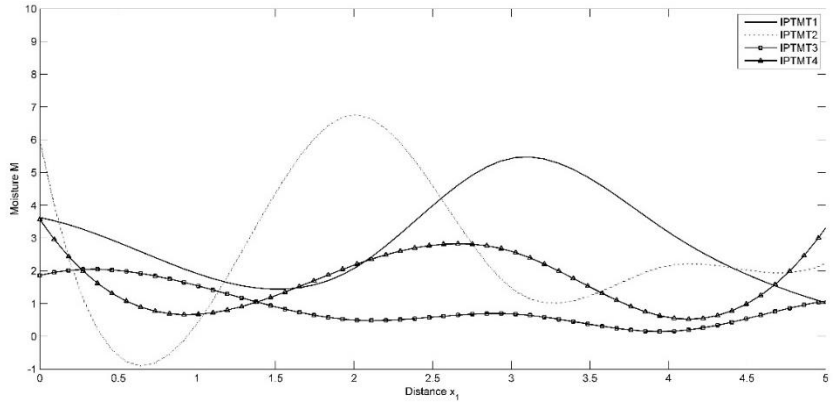


**Fig. 8.** Impact of relaxation times on moisture *M* due to carrier density source

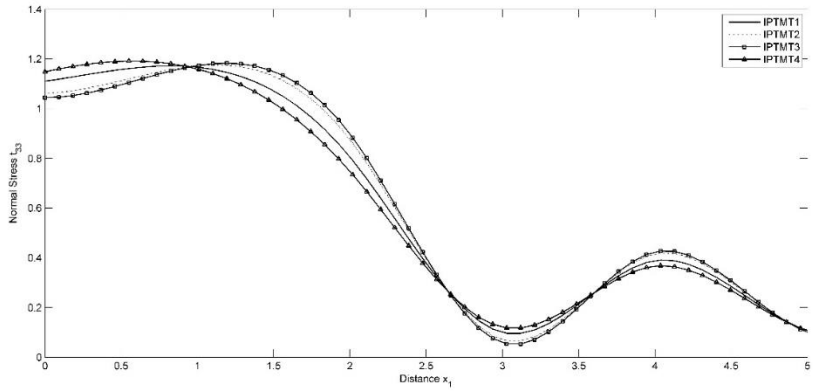


**Fig. 9.** Impact of relaxation times on normal stress $t_{33}$ due to moisture source

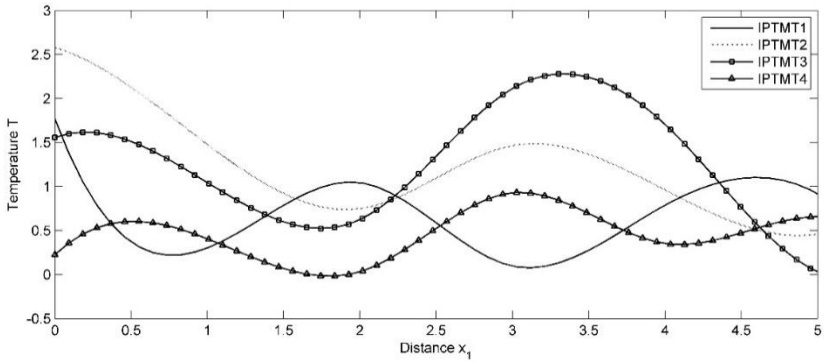


**Fig. 10.** Impact of relaxation times on temperature *T* due to moisture source

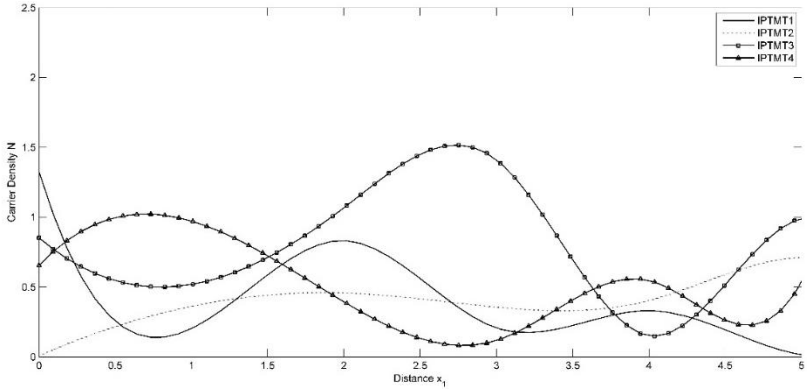


**Fig. 11.** Impact of relaxation times on carrier density *N* due to moisture source

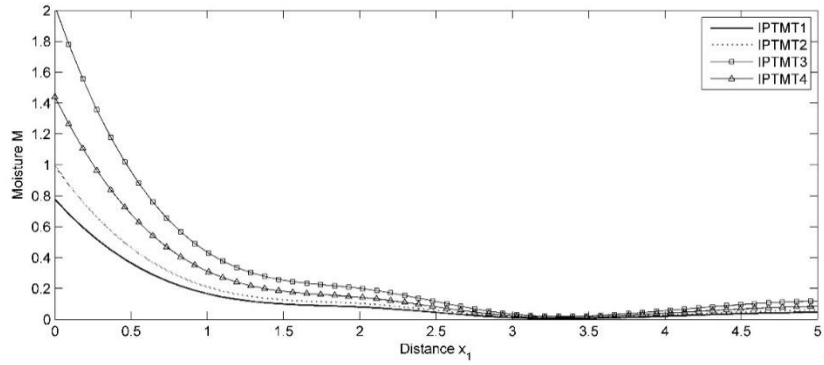


**Fig. 12.** Impact of relaxation times on moisture *M* due to moisture source

Figure 9 displays the variation of normal stress $t_{33}$ with $x_1$. $t_{33}$ exhibits an increasing tendency near the vicinity of the source across all models. With the increasing distance, $t_{33}$ begins to decrease in reverse order and reveals an oscillating tendency with magnitudes varying between models.

Figure 10 shows the variation of temperature $T$ with $x_1$. $T$ for IPTMT1 and IPTMT2 exhibit an initial decline, followed by opposite oscillatory trend in the range $0.75 \leq x_1 \leq 5$. Meanwhile, $T$ for IPTMT3 and IPTMT4 displays a similar oscillatory behavior in the range $0 \leq x_1 \leq 4$, and beyond this range, it transitions into an opposite oscillatory behavior.

Figure 11 illustrates how the carrier density $N$ varies with $x_1$. Close to the source, $N$ for IPTMT1 and IPTMT3 models follow a declining trend, though $N$ for IPTMT2 and IPTMT4 shows an increasing pattern. $N$ for IPTMT3 and IPTMT4 demonstrate more pronounced oscillations compared to IPTMT1 and IPTMT2 models. $N$ for IPTMT1 displays significant oscillations in the range $0 \leq x_1 \leq 3$, and slight oscillation around $3 \leq x_1$. $N$ for IPTMT2 follows an increasing trend in the range $0 \leq x_1 \leq 2$, and maintains a relatively mild oscillatory pattern beyond this range. The oscillatory pattern of $N$ for IPTMT3 and IPTMT4 is opposing with high variation in magnitude.

Figure 12 displays the variation of moisture $M$ with $x_1$. Near the source, $M$ for all the models exhibit a decreasing trend, with the IPTMT3 model showing the highest magnitude and IPTMT1 model the lowest and display slight oscillations within the range $1 \leq x_1 \leq 3$. Near the source, there is a notable difference in magnitude for all the models, while away from the source, the magnitudes tend to converge, and all models exhibit a consistent upward trend, accompanied by slight amplitude variations.

## Conclusions

This study investigates the deformation in an isotropic IPTM plate due to the influence of a carrier density source and a moisture source. General equations are used to derive the governing equations and constitutive relations for the plate under consideration. To simplify the analysis, non-dimensional variables and potential functions are employed. Analytical solutions for the resulting equations are obtained through Laplace and Fourier transforms, and numerical inversion techniques are applied to retrieve the solutions in the physical domain. Graphical representations illustrate the effects of moisture, relaxation times, and source terms on various physical fields such as stress, temperature, carrier density, and moisture distribution. Based on the numerical results, the following key conclusions can be drawn.

*Carrier density source*. The presence of moisture leads to a more stable pattern of normal stress, showing reduced fluctuations. Moisture presence also slightly attenuates temperature variations. Carrier density maintains comparable behavior, with higher magnitude induced by moisture. Moisture content oscillates more strongly with larger thermal and moisture relaxation times ($\tau_o = 0.05$, $\tau^o = 0.04$), near the source. For all models, normal stress display oscillations. Near the source, normal stress reaches higher values, for smaller thermal and higher moisture relaxation times ($\tau_o = 0.03$, $\tau^o = 0.04$). Near the source, Temperature and Moisture fluctuations are more pronounced and attain extremes for higher thermal and moisture relaxation times ($\tau_o = 0.05$, $\tau^o = 0.04$), while at greater distances, stronger fluctuations occur under smaller relaxation times ($\tau_o = 0.03$,

$\tau^o = 0.02$). Carrier density for all models initially decreases monotonically then transitions into a slight oscillatory phase and subsequently shows a modest increase, amplified under smaller thermal and higher moisture relaxation times.

*Moisture source*. Normal stress intensifies near the source, and its peaks and valleys occur at identical positions across all models. It has peaks for lower thermal and higher moisture relaxation times ($\tau_o = 0.03$, $\tau^o = 0.04$) and lower overall magnitude when relaxation effects are absent. Near the source, temperature fluctuations are more pronounced for smaller thermal and moisture relaxation times ($\tau_o = 0.03$, $\tau^o = 0.02$). At greater distances, temperature shows stronger fluctuations with increased magnitude for lower thermal and higher moisture relaxation times ($\tau_o = 0.03$, $\tau^o = 0.04$). Carrier density exhibits pronounced oscillations across the domain under the conditions of high moisture relaxation time ($\tau_o = 0.03$, $\tau^o = 0.04$) and when relaxation times are disregarded ($\tau_o = 0$, $\tau^o = 0$). Moisture concentration undergoes a monotonic decrease in all cases, with higher attenuation magnitude corresponding to lower thermal and higher moisture relaxation times ($\tau_o = 0.03$, $\tau^o = 0.04$). However, with distance, the moisture profile transitions into an oscillatory form that eventually converges, subsequently exhibiting a minor increasing trend.

The proposed method offers a unified analytical approach to study coupled thermoelastic, moisture, and photo-induced effects in semiconducting materials. It is particularly relevant for microelectronic, optoelectronic, and photovoltaic devices, where thermal loading, carrier excitation, and moisture exposure affect performance and reliability. The model aids in optimizing thermal management and structural stability, providing deeper insight into transient behavior under realistic operating conditions.

## CRediT authorship contribution statement

**Rajneesh Kumar**: conceptualization, supervision, literature review, methodology, software, visualization, investigation; **Nidhi Sharma**: assistance in methodology refinement, analysis and interpretation of the study; **Vineeta Rani**: writing, draft preparation, validation and visualization.

## Conflict of interest

The authors declare that they have no conflict of interest.

## References

1. Mandelis A. *Photoacoustic and thermal wave phenomena in semiconductors*. New York: Elsevier Science; 1987.
2. Almond DP, Patel PM. *Photothermal science and techniques*. London: Chapman & Hall; 1996.
3. Nikolic PM, Todorovic DM. Photoacoustic and electroacoustic properties of semiconductors. *Progress in Quantum Electronics*. 1989;13(2): 107–189.
4. Mandelis A, Michaelian KH. Photoacoustic and photothermal science and engineering. *Optical Engineering*. 1997;36(2): 301–302.
5. Todorovic D. Photothermal and electronic elastic effects in micro electromechanical structures. *Review of Scientific Instruments*. 2003;74(1): 578–581.
6. Todorovic D. Plasma, thermal, and elastic waves in semiconductors. *Review of Scientific Instruments*. 2003;74(1): 582–585.
7. Todorovic D. Plasmaelastic and thermoelastic waves in semiconductors. *Journal de Physique IV (Proceeding)*. 2005;125: 551–555.

8. Sharma K. Boundary value problem in generalized thermodiffusive elastic medium. *Journal of Solid Mechanics.* 2010;2(4): 348–362.
9. Sharma S, Sharma K, Bhargava RR. Wave motion and representation of fundamental solution in electro-microstretch viscoelastic solids. *Materials Physics and Mechanics.* 2013;17(2): 93–110.
10. Othman MIA, Lotfy K, Farouk RM. Transient disturbance in a half-space under generalized magneto-thermoelasticity with internal heat source. *Acta Physica Polonica A.* 2009;116(2): 185–192.
11. Marin M, Abbas JA, Kumar R. Relaxed Saint-Venant principle for thermoelastic micropolar diffusion. *Structural Engineering and Mechanics.* 2014;51(4): 651–662.
12. Zenkour AM, Abbas IA. Thermal shock problem for a fiber-reinforced anisotropic half-space placed in a magnetic field via G–N model. *Applied Mathematics and Computation.* 2014;246: 482–490.
13. Lotfy K. Two-temperature generalized magneto-thermoelastic interactions in an elastic medium under three theories. *Applied Mathematics and Computation.* 2014;227: 871–888.
14. Sharma S, Sharma K. Influence of heat sources and relaxation time on temperature distribution in tissues. *International Journal of Applied Mechanics and Engineering.* 2014;19(2): 427–433.
15. Abbas IA, Othman MIA. Plane waves in generalized thermo-microstretch elastic solid with thermal relaxation using finite element method. *International Journal of Thermophysics.* 2012;33: 2407–2423.
16. Hobiny A, Abbas IA. A GN model on photothermal interactions in a two-dimensional semiconductor half-space. *Results in Physics.* 2019;15: 102588.
17. Hobiny A, Abbas IA. Fractional order GN model on photo-thermal interaction in a semiconductor plane. *Silicon.* 2020;12: 1957–1964.
18. Marin M, Hobiny A, Abbas IA. The effects of fractional time derivatives in porothermoelastic materials using finite element method. *Mathematics.* 2021;9(14): 1606.
19. Lotfy K, El-Bary AA. Magneto-photo-thermo-microstretch semiconductor elastic medium due to photothermal transport process. *Silicon.* 2022;14: 4809–4821.
20. Abbas IA. A GN model based upon two-temperature generalized thermoelastic theory in an unbounded medium with a spherical cavity. *Applied Mathematics and Computation.* 2014;245: 108–115.
21. Abbas IA. A GN model for thermoelastic interaction in a microscale beam subjected to a moving heat source. *Acta Mechanica.* 2015;226: 2527–2536.
22. Sharma N, Kumar R. Photo-thermoelastic investigation of semiconductor material due to distributed loads. *Journal of Solid Mechanics.* 2021;13(2): 202–212.
23. Sharma N, Kumar R. Photothermoelastic deformation in dual phase lag model due to concentrated inclined load. *Italian Journal of Pure and Applied Mathematics.* 2022;48–2022: 1147–1160.
24. Lotfy K, El-Bary AA, El-Sharif AH. Ramp-type heating microtemperature for a rotator semiconducting material during photo-excited processes with magnetic field. *Results in Physics.* 2020;19: 103338.
25. Mahdy AMS, Lotfy K, Ismail EA, El-Bary AA, Ahmed M, El-Dahdouh AA. Analytical solutions of time-fractional heat order for a magneto-photothermal semiconductor medium with Thomson effects and initial stress. *Results in Physics.* 2020;18: 103174.
26. Sharma S, Khator S. Power generation planning with reserve dispatch and weather uncertainties including penetration of renewable sources. *International Journal of Smart Grid and Clean Energy.* 2021;10(4): 292–303.
27. Sharma S, Khator S. Micro-grid planning with aggregator's role in the renewable inclusive prosumer market. *Journal of Power and Energy Engineering.* 2022;10(4): 47–62.
28. Lotfy K, El-Bary AA, Hassan W, Ahmed MH. Hall current influence of microtemperature magneto-elastic semiconductor material. *Superlattices and Microstructures.* 2020;139: 106428.
29. Hobiny A, Abbas IA, Marin M. The influences of the hyperbolic two-temperatures theory on waves propagation in a semiconductor material containing spherical cavity. *Mathematics.* 2022;10(1): 121.
30. El-Sapa S, Becheikh N, Chtioui H, Lotfy K, Seddeek MA, El-Bary AA, El-Dali A. Moore–Gibson–Thompson model with the influence of moisture diffusivity of semiconductor materials during photothermal excitation. *Frontiers in Physics.* 2023;11: 1224326.
31. Raddadi MH, Lotfy K, Mahdy AMS, El-Bary AA, Elidy ES. A novel model of photoacoustic and thermalelectronic waves in semiconductor material. *AIP Advances.* 2025;15(1): 015207.
32. Sharma K, Marin M, Kumar R. Thermomechanical deformation in a micropolar thermoviscoelastic solid under the Moore–Gibson–Thompson heat equation with non-local and hyperbolic two-temperature effects. *Journal of Computational Applied Mechanics.* 2025;56(4): 720–736.
33. Szekeres A. Analogy between heat and moisture. *Computers & Structures.* 2000;76(1-3): 145–152.

34. Szekeres A. Cross-coupled heat and moisture transport: Part 1 – Theory. *Journal of Thermal Stresses.* 2012;35(1–3): 248–268.
35. Szekeres A, Engelbrecht J. Coupling of generalized heat and moisture transfer. *Periodica Polytechnica Mechanical Engineering.* 2000;44(1): 161–170.
36. Sih GC, Michopoulos JG, Chou SC. *Hygrothermoelasticity*. Netherlands: Springer; 1986.
37. Alhashash A, Elidy ES, El-Bary AA, Tantawi RS, Lotfy K. Two-temperature semiconductor model photomechanical and athermal wave responses with moisture diffusivity process. *Crystals.* 2022;12(12): 1770.
38. El-Sapa S, Lotfy K, El-Bary AA, Ahmed MH. Moisture diffusivity and photothermal excitation in non-local semiconductor materials with laser pulses. *Silicon.* 2023;15: 4489–4500.
39. Lotfy K, Mahdy AMS, El-Bary AA, Elidy ES. Magneto-photo-thermoelastic excitation of rotating semiconductor medium based on moisture diffusivity. *Computer Modeling in Engineering & Sciences.* 2024;141(1): 107–126.
40. Alshehri HM, Lotfy K. A photo thermoacoustic diffusion model for hydro poroelastic nanocomposite semiconductor medium with chemical potential. *Physics of Fluids.* 2025;37(1): 017121.
41. Kumar R, Devi S. A problem of thick circular plate in modified couple stress theory of thermoelastic diffusion. *Cogent Mathematics.* 2016;3(1): 1217969.
42. Kumar R, Kaushal S, Dahiya V. Porosity and phase lags response of thick circular plate in modified couple stress thermoelastic medium. *ZAMM – Journal of Applied Mathematics and Mechanics.* 2021;101(12): e202100098.
43. Kumar R, Sharma N, Chopra S. Axisymmetric deformation of thick circular plate under Moore–Gibson–Thompson photothermoelastic model. *Advances in Materials Research.* 2025;14(1): 1–30.
44. Abbas IA, Kumar R, Chawla V. Response of thermal source in a transversely isotropic thermoelastic half-space with mass diffusion by using a finite element method. *Chinese Physics B.* 2012;21(8):084601.
45. Abbas IA, Kumar R. Response of thermal source in initially stressed generalized thermoelastic half-space with voids. *Journal of Computational and Theoretical Nanoscience.* 2014;11: 1472–1479.
46. Lotfy K, Elshazly IS, Halouani B, Sharma S, Ailawalia P, El-Bary AA. Influence of Hall current and acoustic pressure on nano-structured DPL thermoelastic plates under ramp heating in a double-temperature model. *Open Physics.* 2025;23(1): 20250125.
47. Alzahrani FS, Abbas IA. Photo-thermo-elastic interactions without energy dissipation in a semiconductor half-space. *Results in Physics.* 2019;15: 102805.
48. Sharma S, Marin M, Altenbach H. Elastodynamic interactions in thermoelastic diffusion including non-local and phase lags. *ZAMM – Journal of Applied Mathematics and Mechanics.* 2025;105(1): e202401059.
49. Alenazi A, Ahmed A, El-Bary AA, Tantawi RS, Lotfy K. Moisture photo-thermoelasticity diffusivity in semiconductor materials: a novel stochastic model. *Crystals.* 2023;13(1): 42.